Alshawaf, F., Zus, F., Balidakis, K., Deng, Z., Hoseini, M., Dick, G., Wickert, J. (2018): On the Statistical Significance of Climatic Trends Estimated From GPS Tropospheric Time Series. - *Journal of Geophysical Research*, *123*, 19, pp. 10,967—10,990.

DOI: http://doi.org/10.1029/2018JD028703

Journal of Geophysical Research: Atmospheres

RESEARCH ARTICLE
10.1029/2018JD028703

On the Statistical Significance of Climatic Trends Estimated From GPS Tropospheric Time Series

F. Alshawaf[1], F. Zus[1], K. Balidakis[1], Z. Deng[1], M. Hoseini[2], G. Dick[1], and J. Wickert[1,3]

[1]GFZ German Research Centre for Geosciences, Potsdam, Germany, [2]Department of Civil and Environmental Engineering, Norwegian University of Science and Technology, Trondheim, Norway, [3]Institute of Geodesy and Geoinformation Science, Technische Universität Berlin, Berlin, Germany

Key Points:
- Climatic trends are estimated from water vapor time series
- GPS tropospheric products are adequately long to be used for climate studies
- The statistical significance of the trends should be estimated based on an autoregressive model rather than a white noise process

Correspondence to:
F. Alshawaf,
fadwa.alshawaf@gfz-potsdam.de

Citation:
Alshawaf, F., Zus, F., Balidakis, K., Deng, Z., Hoseini, M., Dick, G., & Wickert, J. (2018). On the statistical significance of climatic trends estimated from GPS tropospheric time series. *Journal of Geophysical Research: Atmospheres*, *123*, 10,967–10,990. https://doi.org/10.1029/2018JD028703

Received 23 MAR 2018
Accepted 21 SEP 2018
Accepted article online 24 SEP 2018
Published online 9 OCT 2018

Abstract For more than two decades, Global Positioning System (GPS) tropospheric delays have successfully been exploited to monitor the tropospheric water vapor in near real time and reprocessing mode. Although reprocessed data are considered reliable for climatic research, it is important to address the often present gaps, inhomogeneities, and to use a proper model to describe the stochastic part of the time series so that trustworthy trends are estimated. Having relatively long time series, daily reprocessed tropospheric Zenith Total Delay, precipitable water vapor (PWV), and gradients from the Tide Gauge benchmark monitoring network are used in this work to estimate climatic trends. We use a first-order autoregressive model AR(1) to describe the residuals after the trend estimation so that a correct trend uncertainty is estimated. Using the same model, we obtain the number of years of PWV data required to estimate statistically significant trends. For comparison, we produce tropospheric parameters at each Tide Gauge station based on ERA-Interim refractivity fields. We found that 83% of 64 GPS stations show a positive PWV trend below 1 mm/decade independent of the time interval, with approximately half of the trends indicated significant. There is a strong correlation (86%) between the Global Navigation Satellite Systems and ERA-Interim PWV trends. The trends tend to increase when moving east and south on the European map. The results show a percentage change of PWV of 3–8% per a degree Celsius rise in temperature. The number of years required to detect significant PWV trends varies between 30 and 40 years.

1. Introduction

According to the Intergovernmental Panel on Climate Change reports, the scientific evidence for the warming of the Earth's climate system is unequivocal. Since the middle twentieth century, the warming trend is of particular significance because most of it is extremely likely to be anthropogenic. Increasing levels of noncondensing gases, such as carbon dioxide, emitted into the atmosphere cause 25% of the greenhouse effect, while water vapor is responsible for the remaining 75% (Lacis et al., 2010). Water vapor is an active, most abundant component in the climate system that particularly plays a great role in the Earth's warming, which in turn leads to more evaporation and more warming, a positive feedback loop. Atmospheric water vapor content and evaporation rate change rapidly with the changing temperature forming fast feedback processes that accelerate the warming effect compared to the no feedback conditions (Lacis et al., 2010; Ye & Fetzer, 2010). The nonlinear Clausius-Clapeyron relationship predicts the increase of specific humidity at higher air temperatures, which means that global warming will increase the cloud formation and precipitation levels and that the water vapor-related greenhouse effect is more evident in summer under nearly constant relative humidity measurements (Ye & Fetzer, 2010). A lot of effort has been put on estimating and studying climatic trends in water vapor time series from ground- and space-based observing systems as well as reanalysis and model data (Alshawaf et al., 2017; Hausmann et al., 2017; Mieruch et al., 2014; Sherwood et al., 2010; Trenberth et al., 2005). Since the detection of the correct trend depends on its magnitude, the autocorrelation in time series, and its length, it is necessary to identify the statistical significance of the estimated trend. Different studies have put the focus on inspecting the statistical significance of the estimated climatic trends (Mieruch et al., 2008; Santer et al., 2000; Tiao et al., 1990; Weatherhead et al., 1998; Wigley et al., 2006).

Bengtsson et al. (2004) observed an increasing long-term trend with a slope of 0.16 mm per decade in the water vapor data set of ERA-40 within the period of 1958–2001. They suggested applying corrections for the changes in the observing system when using the data for precipitable water vapor (PWV) analysis to achieve

trend values comparable to GPS. ERA-Interim (ERAI) and Modern Era Retrospective-Analysis for Research and Applications have also been used for trend analysis (Simmons et al., 2007; Suarez et al., 2008). Radiosonde and water vapor radiometer were also used to estimate climatic trends (Durre et al., 2009; Trenberth, 2011; Wang et al., 2016).

Despite the vital role of atmospheric water vapor in shaping the climate and weather conditions, the available measurements are still limited in their spatial coverage and the time span might not be adequately long. Reanalysis models assimilate nonhomogenized radiosonde temperature and relative humidity data, which might result in inhomogeneities in the output products (Wang et al., 2016). Global Positioning System (GPS), the first of the Global Navigation Satellite Systems (GNSS), has been used since the 1990s for providing accurate estimates of the atmospheric variables (Alshawaf et al., 2015; Bender et al., 2008; Gendt et al., 2004; Jade & Vijayan, 2008; Luo et al., 2008). As of today, ground-based time series of tropospheric products estimated using geodetic techniques such as GPS and very long baseline interferometry are relatively long and can be used for estimating climatic trends (Alshawaf et al., 2017; Balidakis et al., 2018; Gradinarsky et al., 2002; Haas et al., 2003; Nilsson & Elgered, 2008). The GPS time series are still shorter than the 30-year climate normals defined by climatologists, but this is merely a question of time. Reprocessed GPS tropospheric data have been recommended to be employed for climate studies (Pacione et al., 2017). However, these data, despite being accurate, often have long gaps, inhomogeneities due to hardware changes (Ning et al., 2016; Vey et al., 2009), and outliers; therefore, it is essential to check the quality of the data and select those that are trustworthy for trend estimation. In a preprocessing step, we need to detect and correct for inconsistencies, remove outliers, and infer missing values. It is important to determine the maximum gap length that can be filled without significantly changing the statistical properties of the time series. It might happen, even with a dense GPS network, that only half of the stations (or even less) provide useful data for climate research. In this work we analyzed 193 stations of the Tide Gauge (TIGA) benchmark monitoring network in Europe; 79 of which are available for longer than 10 years. However, due to the presence of long gaps in the time series, only 64 stations proved to be useful for trustworthy trend estimations. For the selected stations, a rigorous assessment of the significance of the trend estimates is indispensable. Therefore, it is essential to use a proper noise model to estimate realistic uncertainty values and hence correct information about the significance of the estimated trends. Since the atmospheric variables show high autocorrelation in daily and monthly time series, a first-order autoregressive model AR(1) introduced by Tiao et al. (1990) or a similar model has to be used to describe the stochastic component of the time series. We analyzed the zenith wet, hydrostatic, total delay, and PWV time series and compared the estimated trends with ERAI-based trends.

We also introduce a method that benefits from the autocorrelation structure of the PWV using the first-order autoregressive model to predict the GPS sample size (in years) of daily data required to estimate statistically significant trends. In addition, we analyze the GPS tropospheric gradient time series to test if they are consistent (correlated) with the spatial distribution of PWV trends.

In this work, we use sufficiently long GPS products for the analysis of climatic trends; however, the research can be extended using products from other GNSS or other observing techniques, when available. We (1) evaluate the quality of the reprocessed GPS-based time series of tropospheric zenith total delay (ZTD), PWV, and gradients in terms of accuracy, homogeneity, and continuity; (2) estimate climatic PWV and ZTD trends and assess their significance based on an AR(1) model; (3) estimate the percentage change with temperature increment; (4) calculate the number of years (length of the time series) required to estimate a significant trend; and (5) estimate the trends in tropospheric gradient time series and compare them to ZTD trends.

This paper is organized as follows. In section 2, we briefly describe the data sets and methods for reprocessing the GPS data to produce the ZTD and zenith wet delay (ZWD). We also introduce the ray tracing of ERAI 3-D fields for deriving ZTD, zenith hydrostatic delay (ZHD), and ZWD and tropospheric gradients at the GPS stations. In section 3, we present the methods for preprocessing the time series in preparation for trend estimation. Then, we describe the method to estimate the trend and quantify its significance. Following is the description of the method used to obtain the required data size in years to estimate a specific trend. In section 4, the results are presented followed by our conclusions of the current research and recommendations for future work.

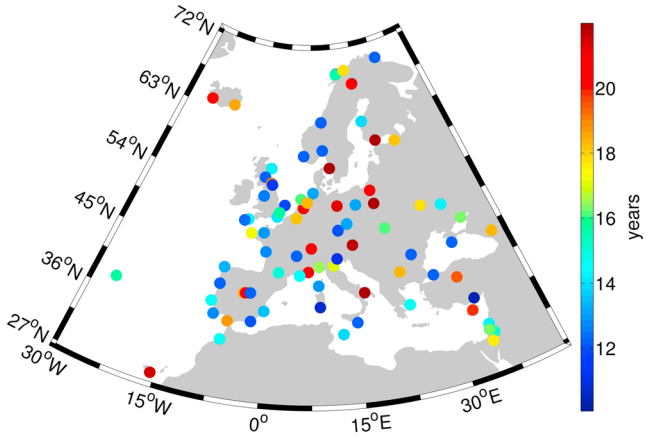

Figure 1. The length of the available Global Positioning System Tide Gauge stations distributed over Europe. The longest time interval extends from 1994 to 2016.

2. Research Region and Data Sets

The trend analysis presented in this paper was done using GPS, ERAI data, and measurements from synoptic stations.

2.1. GPS Data

The International GNSS Service TIGA benchmark monitoring working group is responsible for analyzing GPS data from stations in the vicinity to TIGAs on a preferably continuous basis to provide information about the vertical rates (Schöne et al., 2009). The TIGA network has over 750 globally distributed stations. The station coordinates and vertical velocity results can be exploited for several geodetic and geophysical studies such as global and regional sea level change estimations, calibration of satellite altimeters, and unification of height systems. As one of the TIGA Analysis Centers, the German Research Center for Geosciences (GFZ) is contributing to the International GNSS Service TIGA Reprocessing Campaign (Deng et al., 2015). After the first reprocessing presented in 2010, several improvements were implemented into the latest GFZ software version EPOS.P8 to improve the quality of the derived products. For more details about the models and algorithms used for the reprocessing of GPS TIGA data, the reader is referred to Deng et al. (2015). Besides positions and velocity rates, tropospheric ZTD and gradients are also estimated by reprocessing the GPS data of the global TIGA network. The ZTD and ZWD are estimated hourly, while one tropospheric east-west (EW) and north-south (NS) gradient is estimated per day. For our trend analysis we use daily data that are obtained by averaging the hourly data. Ruffini et al. (1999) showed that the estimated tropospheric EW and NS gradients should roughly be proportional to the spatial ZTD gradients as we explain in Appendix A, and hence, we also apply the trend estimation method to the gradient time series to test whether we can obtain information that supports the ZTD trends. In this paper, we put the focus on the 193 stations in Europe, where the 79 GPS stations that are operating for more than 10 years are shown in Figure 1.

2.2. ERAI Reanalysis Data

As a reference, we used ERAI data (Dee et al., 2011) to derive the corresponding delay components, ZTD, ZHD, ZWD, and the tropospheric EW and NS gradients at each GPS TIGA station at the ERAI temporal resolution. The ERAI is a 6-hourly reanalysis product with a horizontal resolution of 79 km × 79 km on 60 vertical model levels. For the period 1996–2014, the ZWD (also converted into PWV), ZHD, and tropospheric EW and NS gradients were computed at the 193 TIGA stations in Europe using the in-house GFZ ray tracing software (Zus et al., 2012). The ZWD and ZHD are obtained by integrating the nonhydrostatic and hydrostatic atmospheric refractivities, respectively. Then the ZTD is obtained by the sum of both components, that is,

$$\begin{aligned} \mathrm{ZTD}(x,y,t) &= \mathrm{ZHD}(x,y,t) + \mathrm{ZWD}(x,y,t) \\ &= 10^{-6}\left(\int_z N_h(x,y,z,t)\,\mathrm{d}z + \int_z N_w(x,y,z,t)\,\mathrm{d}z\right) \end{aligned} \tag{1}$$

where N_w and N_h are the nonhydrostatic (wet) and hydrostatic atmospheric refractivities. While the ZTD corresponds to a single tropospheric delay in zenith direction, the tropospheric gradients are derived from a set of uniformly distributed tropospheric delays. For details, the reader is referred to Douša et al. (2016). The ZHD (in meters) is linearly related to the air pressure as follows:

$$\mathrm{ZHD} = \frac{0.002277P}{1 - 0.0026\cos 2\phi - 0.00028\mathrm{H}} \tag{2}$$

where H is the orthometric height in kilometers and ϕ is the latitude of the station. P is the corresponding air pressure at the station in hectopascals. The ZWD can be converted into PWV in millimeters using the conversion factor Q presented by Bevis et al. (1992), that is,

$$\mathrm{PWV} = \mathrm{ZWD}/Q \tag{3}$$

with Q, which varies in Europe between 6.1 and 6.5 (Webley et al., 2002), is calculated using the water vapor weighted mean temperature of the atmosphere (Alshawaf et al., 2017).

For our trend analysis, we use daily time series; therefore, both hourly GPS and 6-hourly ERAI data were averaged to a daily temporal resolution. We compared the time series of the ZTD, PWV, and gradients obtained

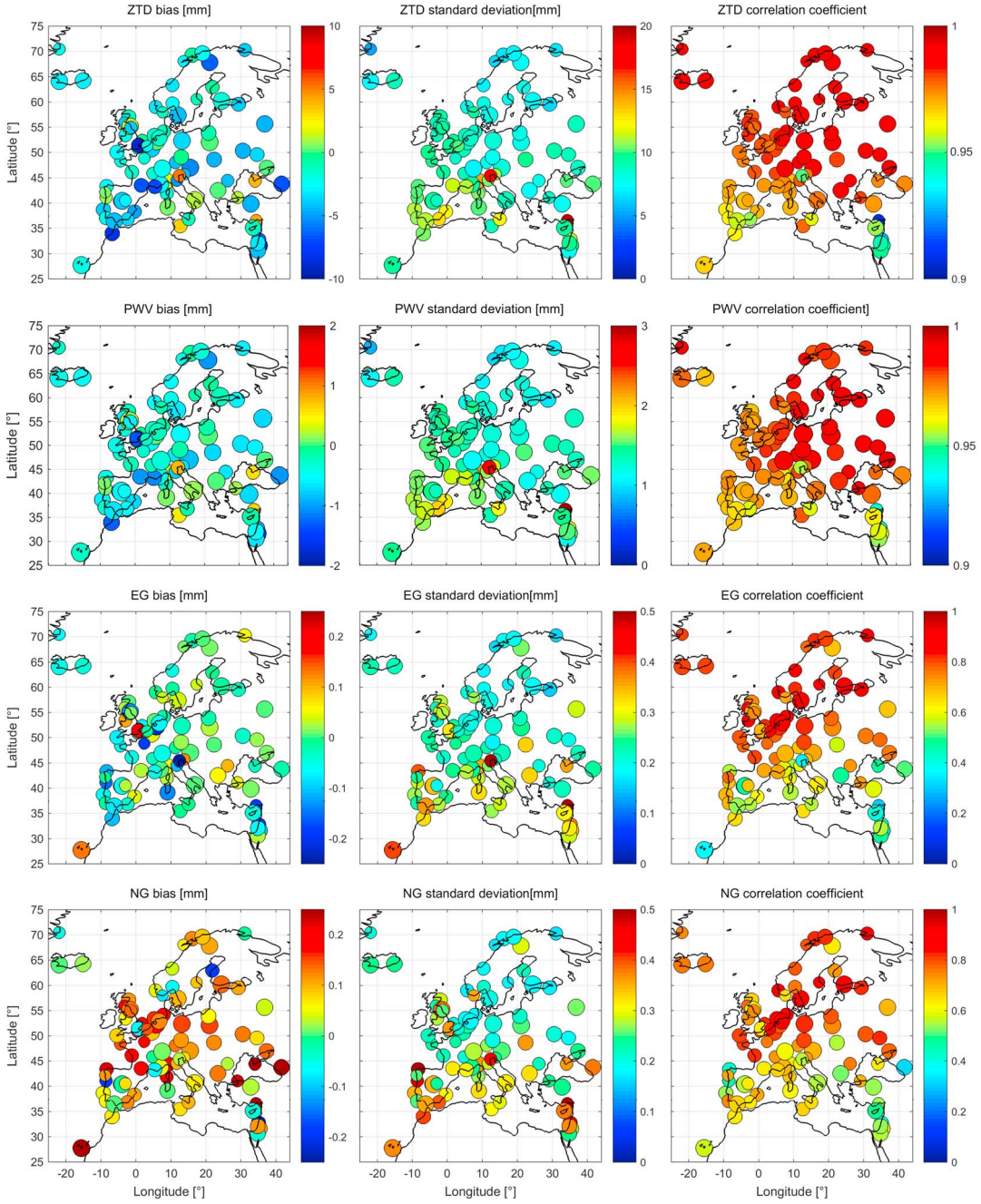

Figure 2. Statistical comparison between GPS ZTD, PWV, EW gradient (EG), and NS gradient (NG) time series with the corresponding from ERAI (GPS-ERAI). GPS = Global Positioning System; ZTD = zenith total delay; PWV = precipitable water vapor; EW = east-west; NS = north-south; ERAI = ERA-Interim.

from ERAI with the GPS estimates, and the results are shown in Figure 2. The difference in ZTD (GPS-ERAI) shows mainly negative bias values, which indicate that the ERAI-based ZTD values are higher. This bias is consistent with the bias reported by, for example, Pacione et al. (2017), but the reason for this bias is still unknown. The observed biases, however, do not exceed 1 cm with standard deviations mainly below 1.5 cm. For PWV, the bias is generally below 1 mm. The two data sets show a strong linear correlation with correlation coefficients above 0.9. The gradients, however, show less strong correlation, particularly in the south (Mediterranean Basin), which is expected because the accuracy of atmospheric models and reanalysis data worsens when moving toward the equator. The standard deviations of the differences (GPS-ERAI) of both gradients are also higher in the south. Since water vapor is not evenly distributed over the globe, the highest amount is

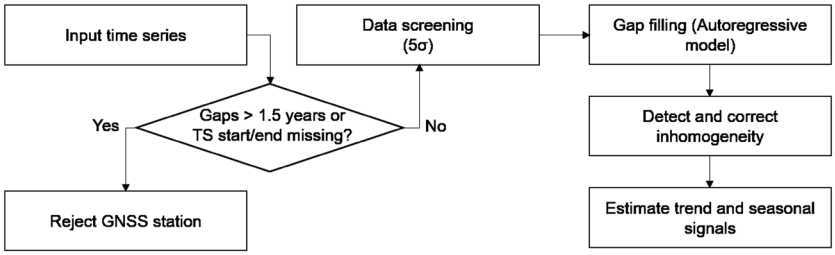

Figure 3. Steps for preparing the time series for climatic trend estimation. GNSS = Global Navigation Satellite Systems.

found near the equator and it decreases when moving toward the poles. This generally holds for the temporal variability of the PWV content, where closer to the equator the PWV shows high variations over hours, or even a shorter time scale, and hence, it is more challenging for the weather models to provide accurate PWV data that capture the actual variations. The higher magnitude of PWV near the equator implies that larger error should be expected, while at the poles the opposite happens. This results in the higher standard deviation and lower correlation coefficient values for ZTD, PWV, and gradients differences when moving south in Europe (in the equator's direction). We observed that the GPS time series generally show higher temporal variability. Due to the coarse spatial resolution, small-scale variation cannot be resolved in ERAI. GPS, however, uses 1 hr of data to estimate the corresponding atmospheric parameters, so the effect of temporal averaging in GPS data is smaller than that in ERAI. In particular, the GPS-derived NS gradient component is larger than the north gradient component from the ERAI. This bias is introduced due to the fact that different gradient mapping functions were used; the gradients from ray tracing ERAI are derived using the gradient mapping function proposed by Chen and Herring (1997), whereas the GPS gradients are derived using the gradient mapping function proposed by Bar-Sever et al. (1998). The Bar-Server mapping function is larger than Chen and Herring's because in the former a part of the asymmetric delay is described by the weather-dependent wet mapping function. This bias is smaller in EW gradient since it depends on the weather conditions, while the NS gradient depends on the thickness of the atmospheric layer, which decreases toward the pole. Because both NS gradients are negative in the the Northern Hemisphere and Bar-Server mapping function is larger, the resulting bias is positive. For more details on the influence of modeling and parameterization on the tropospheric delay, the reader is referred to Balidakis et al. (2018).

3. Climatic Trends

The magnitude of the GPS-based atmospheric parameters such as ZTD and ZWD is dependent of the atmospheric PWV content. The time series of these parameters might show a deterministic change over time that can be described by a linear trend, which can be analyzed to provide information about changes in the Earth's climate. The trends in each of the atmospheric variables ZTD, ZHD, and ZWD in equation (1) are obtained by taking the derivative of all terms with respect to time, that is,

$$\begin{aligned}\frac{\partial \mathrm{ZTD}}{\partial \mathrm{t}} &= \frac{\partial \mathrm{ZHD}}{\partial \mathrm{t}} + \frac{\partial \mathrm{ZWD}}{\partial \mathrm{t}} \\ &= \frac{\partial \mathrm{ZHD}}{\partial \mathrm{t}} + \frac{\partial Q \cdot \mathrm{PWV}}{\partial \mathrm{t}}\end{aligned} \tag{4}$$

Since the ZHD is dependent of the air pressure, which is expected to have no trends, the ZWD trend should equal the ZTD trend. Hence, when assuming that $\partial Q/\partial t$ is negligible and dividing the ZTD trend by the factor Q (say roughly $Q = 6.5$), we will approximately obtain the PWV trend. However, we found that the ZHD time series can have a linear trend; therefore, we need to estimate the trend in the ZTD, ZWD, and ZHD time series in order to draw reasonable conclusions. We used the data sets from GPS and ERAI presented in the previous section to analyze possible climatic effects in Europe. The statistical analysis of the data sets presented above is not adequate to define whether a data set is useful for estimating a trustworthy climatic trend or not. There are different factors that should be considered if we want to estimate climatic trends from the GPS tropospheric products or any data set: the time span of the available time series, its homogeneity, the presence of gaps (particularly at the start and the end of the time series), and the presence of noise and its magnitude compared to the magnitude of the expected trend, the autocorrelation in the time series. It is also essential to identify the significance of the estimated trends. Some environmental variables, because of their low temporal variability and autocorrelation, allow for an early detection (from shorter time series) of the trend than

Table 1
For ERAI PWV Time Series: Mean, SD, 1-Lag Autocorrelation, Trend, and Standard Error Values Obtained With and Without Gap Filling

ERAI PWV	Mean (mm)	SD (mm)	1-Lag Corr.	Trend (mm/decade)	SE (mm)
No gaps	15.17	6.85	0.65	0.54	0.19
400-day gap	15.17	6.83	0.65	0.57	0.19
800-day gap	15.14	6.77	0.66	0.64	0.20

Note. ERAI = ERA-Interim; PWV = precipitable water vapor; SD = standard deviation; SE = standard error.

others (Weatherhead et al., 1998). We want to estimate the trends for the stations in Figure 1, which should have time series longer than 10 years; however, a preprocessing step is required to assess the quality of the time series in terms of the presence of inconsistencies, gaps, and outliers. Although some of the stations have more than 22 years of data, the GPS time span is still rather short, especially in light of the fact that the climatologists define climate norms of 30 years; however, the length of the GPS data is only a question on time. This analysis can show that GPS estimates of atmospheric products have a great potential for providing accurate climatic information when they have the adequate length (Alshawaf et al., 2017; Nilsson & Elgered, 2008). We provide not only the trend magnitude but also its significance, where a trend would not be indicated significant if the time series is not adequately long. In addition, we used these time series to predict the number of years of GPS data required to detect significant trends.

In the following subsections, we describe the preprocessing steps to prepare the time series for trend estimation, the method to estimate the trend and its significance, and the way to calculate the number of years required to detect a specific trend in tropospheric products with a confidence higher than 95%.

3.1. Prepocessing of Time Series

The optimal scenario for the trend estimation is to have an accurate, continuous time series. However, the presence of gaps in GPS-based time series is so far unavoidable due to the absence of raw data or temporary loss of communication with the station owing to hardware-related problems. Therefore, the first step in Figure 3 is to check the length of the gap (the missing data). The trend can, of course, be estimated in the presence of gaps, but we need to check the homogeneity of the time series before the trend estimation and the gap filling step is necessary for any homogeneity check algorithm. Also, the trend magnitude changes in the presence of gaps, especially the beginning or the end of the time series, and longer gaps might result in a very different trend estimate even with applying the gap filling. The gap filling algorithms might not achieve an accurate prediction of the missing data when the gap is extremely long. For these reasons, we reject the stations that have data gaps of longer than 1.5 years. This threshold was selected such that the estimated trend of PWV is not significantly affected by the gap filling. Table 1 shows the mean, standard deviation, trend, and standard error values obtained with and without gaps in the PWV time series (here ERAI was used and the gaps were synthetically induced). As we see in the table, the values in the first (no gaps) and second rows (400 days gap) show almost no differences, while when the gap width increases (800 days) the statistical properties of the time series slightly change as well as estimated trend. Since both the start and end of the time series are crucial for the trend estimate, the stations with missing data at the beginning or end of the time series are also rejected. From the 79 TIGA stations we processed in Europe, 48 stations have no gaps, while 10 stations are

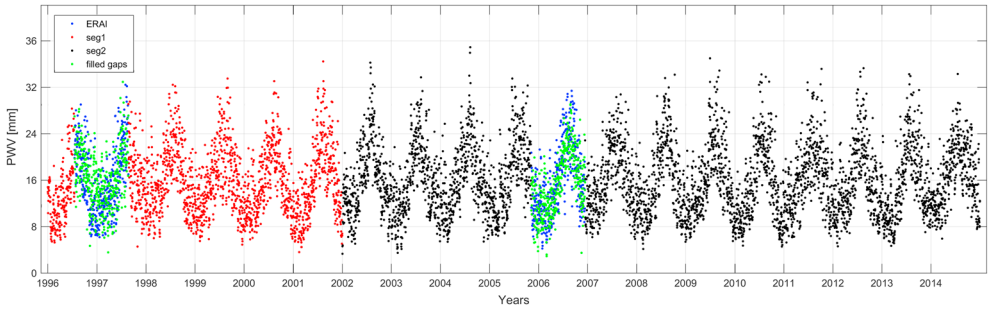

Figure 4. The gap filling is applied by subdividing the time series into two segments, red and black. The first gap is filled using a backward autoregressive model, while the second by a weighted model. PWV = precipitable water vapor; ERAI = ERA-Interim.

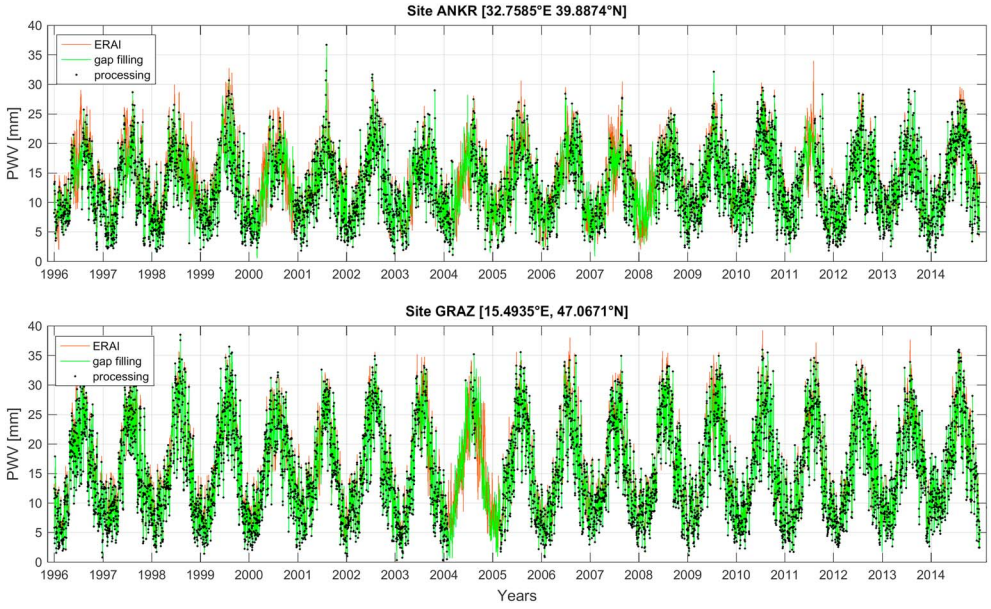

Figure 5. Temporal gaps in the GPS PWV time series are filled using a weighted autoregressive model. GPS = Global Positioning System; PWV = precipitable water vapor; ERAI = ERA-Interim.

missing less than 1 year of data (scattered gaps) in more than 10 years intervals. Two of the stations have gaps longer than 1 year (sequential) and four stations have scattered, longer than 1-year gaps. Fifteen stations that have longer gaps were not further used in the trend estimation.

For the selected 64 GPS stations, data screening is applied to remove data points with five standard deviations from the mean. This threshold was selected because some weather conditions lead to high fluctuations in the PWV and hence the ZWD and ZTD. These fluctuations can correspond to estimates with five standard deviations from the mean. The next step is to fill the gaps in the time series, if the time series has any. For the gap filling, we fit an autoregressive model described in (Akaike, 1969) to the available data and use the fitting to replace the missing data. When the time series has multiple long gaps (longer than 180 days each), we split the time series into segments and perform the prediction based on a forward autoregressive model or backward model or a weighting of forward and backward directions depending on the location of the gap in the addressed segment. An example is shown in Figure 4, where the PWV time series has two gaps (manually induced) and was subdivided into two segments to recover the missing data. For the gap in the first segment (red dots), a backward autoregressive model, is applied to infer the missing data, while a weighted model is applied to fill the gap in the second segment (black dots). This method succeeds in filling the gaps in ZTD, PWV, and gradient time series. Two examples of predicting the missing data and filling the gaps in GPS-based PWV compared to the continuous ERAI PWV time series are exhibited in Figure 5. The final step of this preprocessing scheme is to detect and correct inhomogeneities in the time series. We are applying the

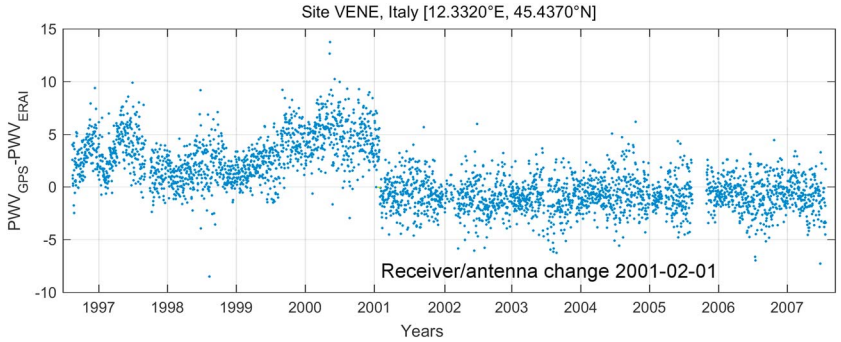

Figure 6. Inconsistency in the PWV time series due to the change in the station receiver and antenna. PWV = precipitable water vapor; GPS = Global Positioning System; ERAI = ERA-Interim.

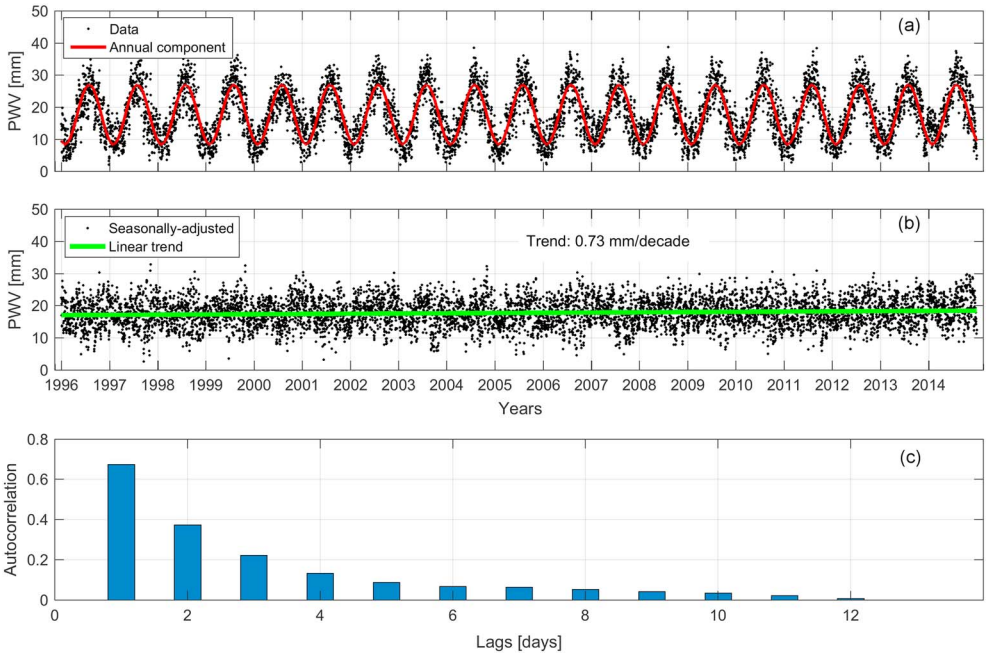

Figure 7. (a) PWV time series at station ABER (2.0802°W, 57.144°N) and annual seasonal component. (b) Seasonally adjusted time series and a linear trend fitting. (c) Autocorrelation of the residuals after removing the seasonal and the trend components. PWV = precipitable water vapor.

homogeneity check using a single time series, that is, no reference time series; hence, it is required to model and remove the seasonal component by fitting the function in equation (7). For detecting the change points in the time series, we used the method presented by Lavielle and Teyssiere (2006) and Killick et al. (2012). Seven of the 64 stations show inhomogeneities related to the change of receiver and antenna as confirmed by the station log files. Figure 6 shows the discrepancies at two of these stations.

3.2. Trend Estimation

A time series trend model of the following form is often used and considered adequate (Tiao et al., 1990):

$$Y = T + S + N \tag{5}$$

where Y is, for example, the PWV time series. T represents the linear trend component,

$$T = a + bt \tag{6}$$

with b the slope of the fitted line, that is, the magnitude of the linear trend and a is the y intercept. S is the seasonal component, with annual period, and N is the high-frequency signal that captures the weather variations in addition to possible noise effects. For the produced gap-free time series, the seasonal component has no impact on the climatic trend and should be reduced from the data. Hence, we first estimate the seasonal components, annual and semiannual, by fitting the following function to the time series:

$$S = \beta_1 \sin\left(\frac{2\pi t}{p}\right) + \beta_2 \cos\left(\frac{2\pi t}{p}\right) \tag{7}$$

with p equals 365.25 days for the annual seasonal component and 183 days for the semiannual component of daily time series. The linear trend is estimated by least squares adjustment from the seasonally adjusted time series, $Y_{\text{ad}} = Y - \hat{S}$. Figures 7a and 7b show an example of PWV times series, the seasonal component, the seasonally adjusted time series, and the linear trend. In order to provide the uncertainty in the trend, it is important to inspect the N component (residuals). If N is assumed to follow a white noise process, the precision σ_b of the estimated trend, b, is obtained from the following:

$$\sigma_b^* = \frac{\sigma_N}{\sqrt{\sum_n (t-\bar{t})^2}} \approx \frac{\sqrt{\sum_n (Y_{\text{ad}} - \hat{T})^2/(n-2)}}{\sqrt{\sum_n (t-\bar{t})^2}} \tag{8}$$

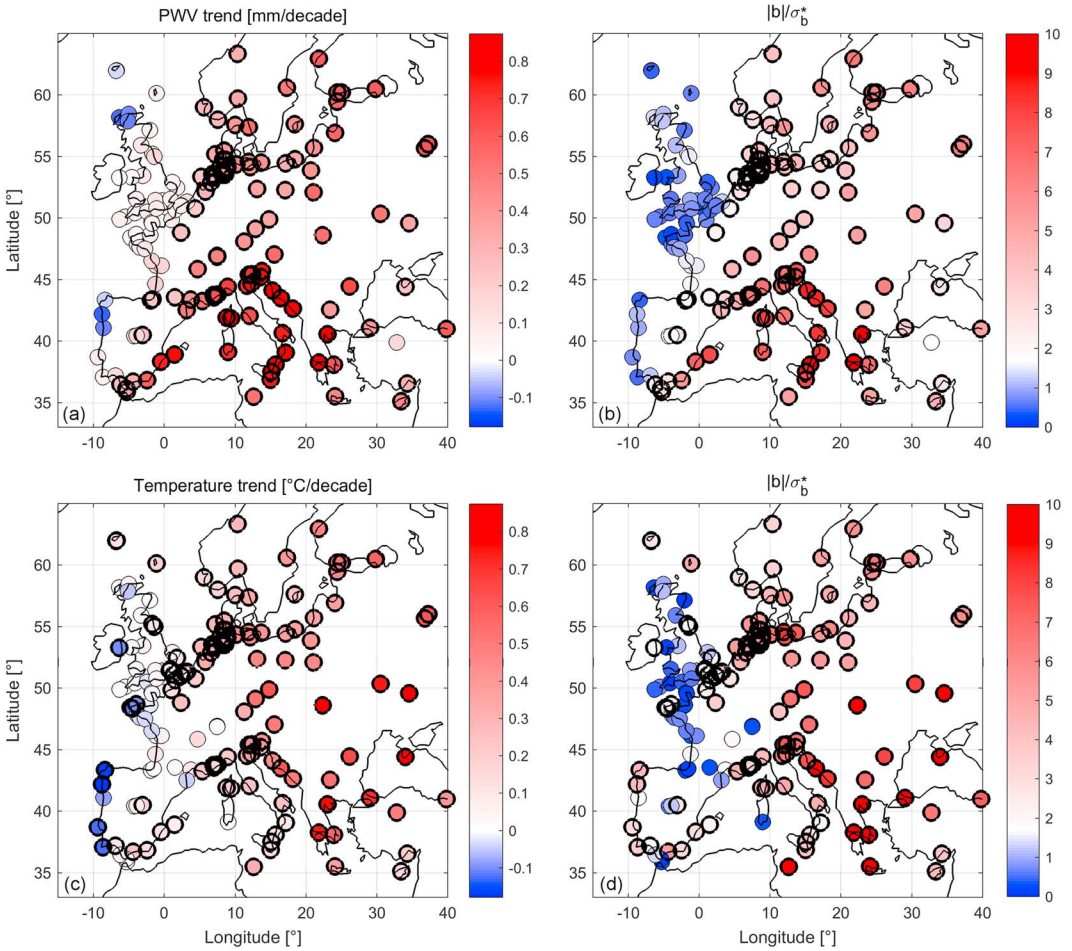

Figure 8. Trend magnitudes estimated from 19-year ERAI-based PWV time series (1996–2014) and the ratio between the estimated trend and the standard error calculated without considering the 1-lag autocorrelation. Stations with statistically significant trend estimates, ratio > 2 indicates, are encircled in black. ERAI = ERA-Interim; PWV = precipitable water vapor.

where σ_N^2 is the variance of the residuals after reducing the deterministic components in equation (5), which corresponds to the high-frequency component *N*. The *n* is the sample size of the data available at time *t* and $\bar{t}$ denotes the mean value. σ_b is also called the standard error. The star symbol is added to indicate the assumption of a white noise process. The larger the standard error, the more uncertain is the slope of the fitted line. We indicate the estimated trend statistically significant at a 0.05 significance level (or 95% confidence level). Should the probability of the null hypothesis, zero trend, be below the significance level (unlikely to be true), the estimated trend is indicated statistically significant. In a similar manner, given the ratio $|b|/\sigma_b$, the null hypothesis is rejected and the trend is indicated as statistically significant at a large ratio (greater than 2, for a confidence level of 95%).

Most of climate data are adequately described by a first-order autoregressive process (Tiao et al., 1990; Wigley et al., 2006). Therefore, climate time series are expected to show significant autocorrelation at least at 1-lag (temporal shift), particularly when daily data are used, as shown in Figure 7c. This figure shows the autocorrelation of the residuals ($Y_{ad} - \hat{T}$), which is highest at 1-day lag and continues to decrease until zero. The location of the station at which the tropospheric parameter is estimated determines the temporal lag at which the time series shows positive autocorrelation. The high-frequency component of, for example, the PWV time series shows positive autocorrelation up to 2 weeks in midlatitudes and up to 60 days in the equatorial region. Since the autocorrelation affects the size of effective sample, that is, $n_{\text{eff}} = n \cdot \left(\frac{1-r_1}{1+r_1}\right)$ (Wigley et al., 2006), it has to be considered when analyzing the significance of the estimated trend. Tiao et al. (1990) suggested the following first-order autoregressive with white noise AR(1) model, which has been useful to describe the

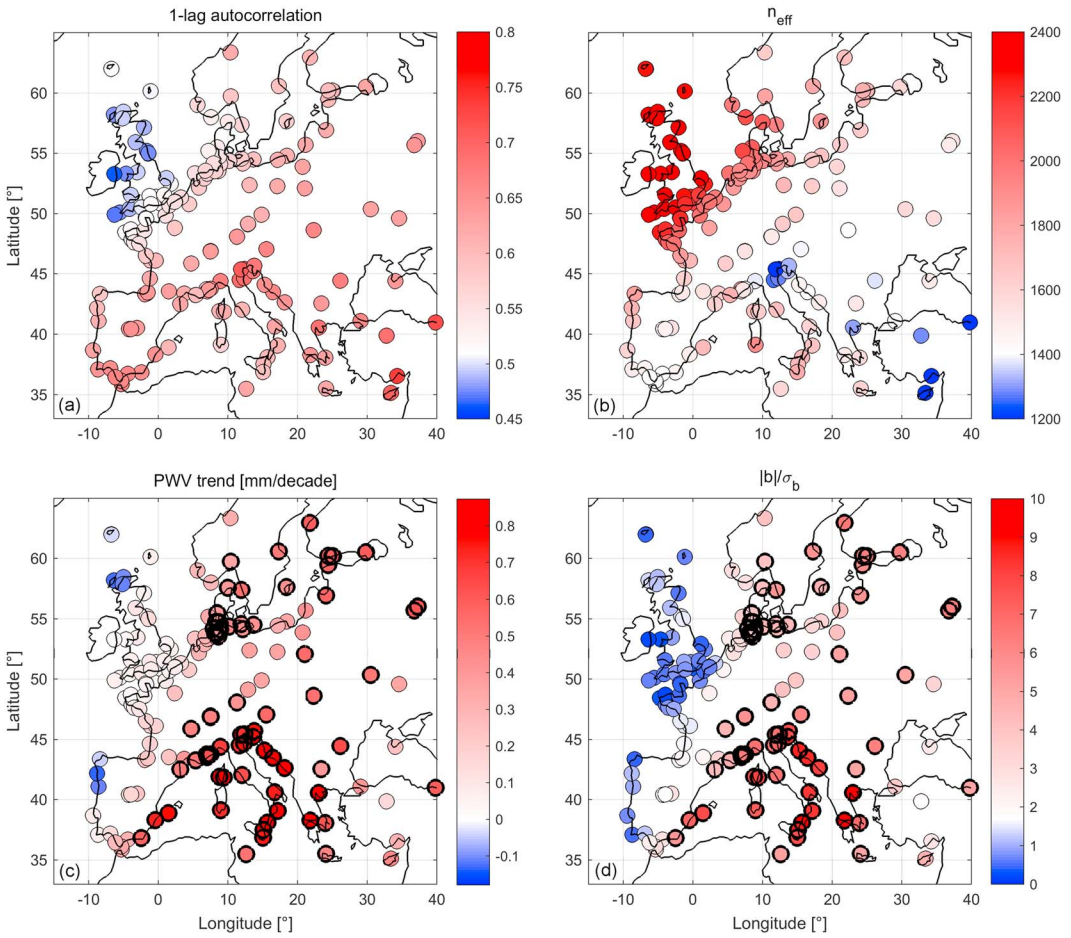

Figure 9. (a) The 1-lag autocorrelation coefficient. (b) Effective number of sample of the available 6940 ERAI data points (1996–2014). (c) Estimated trend with the number of significant estimates reduced since in (d) the standard error, and hence the ratio to the estimated trend, is obtained by including the 1-lag autocorrelation in the calculations. ERAI = ERA-Interim; PWV = precipitable water vapor.

autocorrelation in atmospheric data:

$$N_t = r_1 N_{t-1} + \epsilon_t \tag{9}$$

with r_1 the 1-lag autocorrelation coefficient, that is, the first-order autoregressive coefficient estimated from equation (A4) (Santer et al., 2000; Tiao et al., 1990) and the error term ϵ_t represents a white noise process. Therefore,

$$\sigma_N^2 = \frac{\sigma_\epsilon^2}{(1 - r_1^2)} \tag{10}$$

In the presence of the autocorrelation, the standard deviation (standard error) of the estimated trend (equation (8)) becomes

$$\sigma_b = \frac{\sigma_N}{\sqrt{\sum_n (t - \bar{t})^2}} \cdot \sqrt{\frac{1 + r_1}{1 - r_1}} \tag{11}$$

This equation is derived in Appendix A. It is noted that the value of σ_b as estimated from equation (11) increases when using the autoregressive model in equation (9) rather than a simple white noise; therefore, $\sigma_b = \sqrt{\frac{1+r_1}{1-r_1}}\sigma_b^*$. It is observed from equation (11) that the trend uncertainty increases for higher σ_N or autocorrelation, while the uncertainty decreases when the data size (n) increases. Since σ_b directly affects the confidence interval, that is, higher standard errors result in less confidence (the probability of the null hypothesis increases). This means it is likely that a trend estimate is indicated as statistically significant when neglecting the 1-lag autocorrelation (white noise model, equation (8) but indicated as not statistically significant when including r (AR(1) model, equation (11).

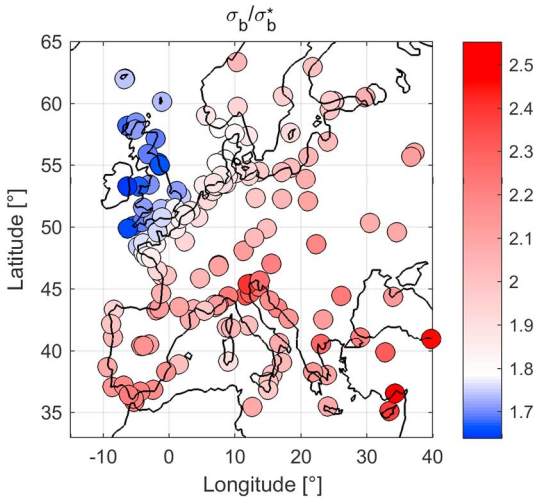

Figure 10. The ratio between the trend standard errors σ_b and σ_b^* with and without using the AR(1) model, respectively.

Since the ZTD is the sum of ZHD and ZWD, which is proportional to the PWV, we want to estimate the linear trend in the ZTD or ZWD time series. Assuming that the ZHD has a zero trend, the ZTD or the ZWD trend should be related to the water vapor trend by the factor Q in equation (3). We will see, however, that the ZHD has a nonzero trend, though small, and hence should be considered when we want to estimate the PWV trend from the GPS-based tropospheric delay time series.

3.3. Sample Size and Trend Detection

If the real trend is small and the magnitude of variability in the deseasonalized signal is large, it may require a very large sample to distinguish the trend from the background noise (Wigley et al., 2006). Then, it is of interest is to determine the number of years of daily or monthly data required to detect a trend of a certain magnitude at a given significance level (Tiao et al., 1990; Weatherhead et al., 1998). The detection of long-term trend is affected by the length of the time series, the magnitude of temporal variations, the presence of autocorrelation in the high-frequency component (N), and the magnitude of the trend to be detected. According to Tiao et al. (1990), the required size of monthly data can be obtained from the following relation:

$$n_{req} = \left[3.3 \, \frac{\sigma_N}{|b_o|} \sqrt{\frac{1+r}{1-r}} \right]^{2/3} \tag{12}$$

where n_{req} is the number of years required to derive a trend of magnitude b_o in millimeters per year from monthly data at a 90% confidence level and σ_N is given in millimeters. We replace the factor 3.3 in the above equation by 3.64 achieve 95% confidence, that is, $n_{\text{req}} = [\, 3.64 \, (\sigma_N/|b_o|) \, \sqrt{(1+r_1)/(1-r_1)} \,]^{2/3}$. We extended

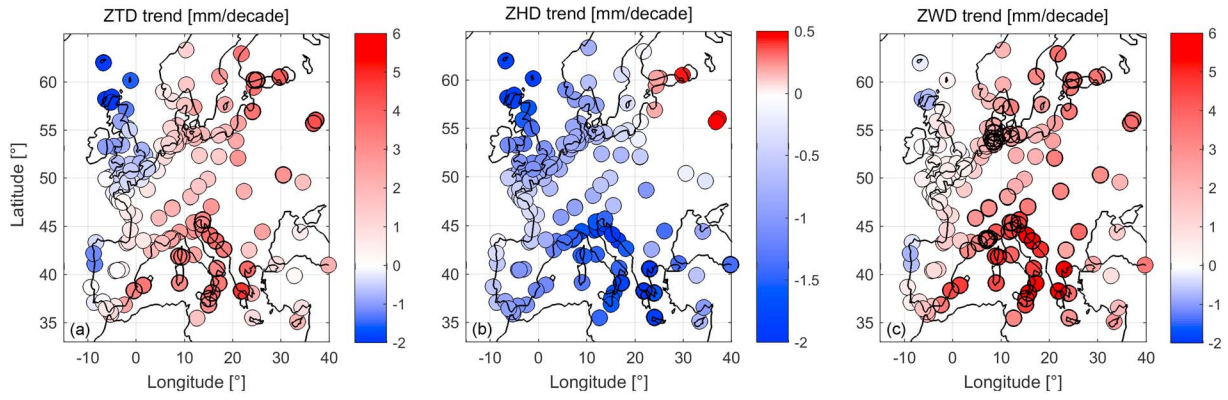

Figure 11. (a–c) Magnitude of linear trends estimated from ZHD, ZWD, and ZTD time series. The 19-year time series (1996–2014) from ray tracing ERAI data were used. Black circles indicate statistically significant trends. ZHD = zenith hydrostatic delay; ZWD = zenith wet delay; ZTD = zenith total delay; ERAI = ERA-Interim.

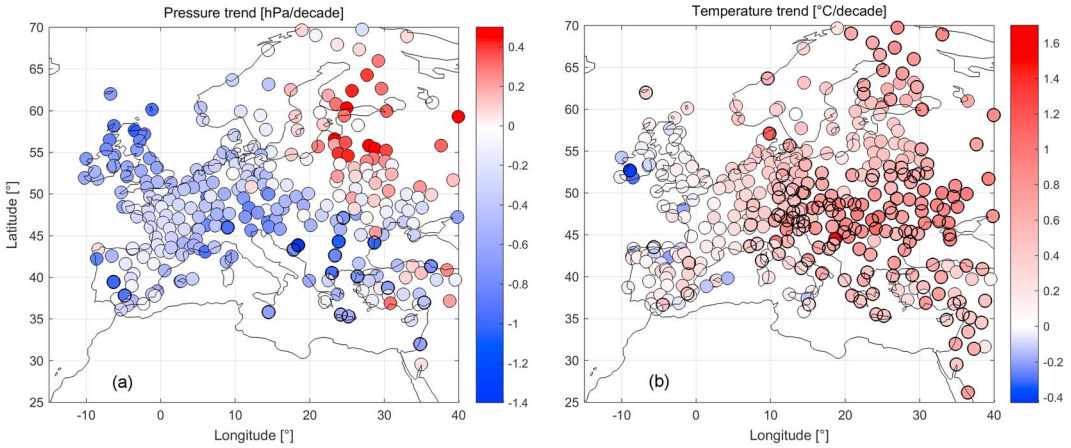

Figure 12. (a, b) Magnitude of linear trends estimated from 19-year (1996–2014) pressure and temperature homogenized time series. Black circles indicate statistically significant trends.

the relation to daily data, and the formula for obtaining the required number of years of daily data slightly differs from equation (12), that is,

$$n_{\text{req}} = \left[3.3 \frac{\sqrt{12}}{\sqrt{365.25}} \frac{\sigma_N}{|b_o|} \sqrt{\frac{1+r_1}{1-r_1}} \right]^{2/3} \tag{13}$$

where trends b_o and σ_N are given in millimeters per year and millimeter, respectively. The derivation of n_{req} is shown in Appendix A. From equations (12) and (13), we can notice when keeping other parameters constant that small σ_N, namely, smooth temporal variations in time series, reduced the required size of the time series. When the time series has high fluctuations, the required size will increase, particularly when the detected trend b_o is small. Higher values of 1-lag autocorrelation also mean that longer time series will be needed to detect a specific trend.

4. Results

4.1. Tropospheric Delay Trends

4.1.1. ERAI Time Series

We started the time series analysis with the ERAI data since they have a uniform length and are available at the 193 TIGA stations in Europe. After checking their homogeneity, we estimated the magnitude of the trend in millimeters per decade from the 19-year PWV time series (1996–2014) by applying least squares adjustment to the seasonally adjusted time series (annual and semiannual seasonal components removed). To check the significance of the estimated trends, we calculated the ratio $|b|/\sigma_b^*$ with the 1-lag autocorrelation not considered when calculating σ_b^*; that is, the residuals after the trend estimation are assumed to follow a white noise distribution. The results are shown in Figure 8. Mainly, the data at stations on the Atlantic coast (45%) yield not

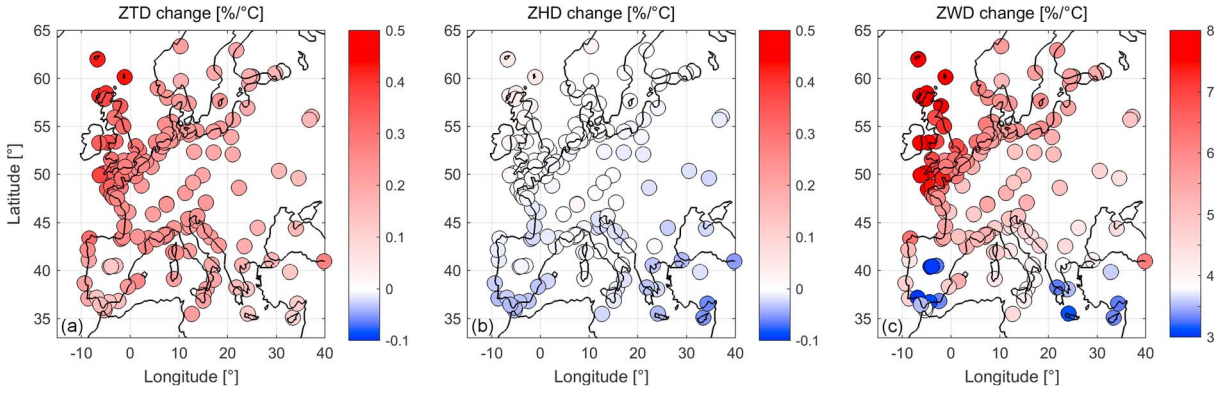

Figure 13. The percentage change of ZTD, ZHD, and ZWD per 1° C increase in temperature. ZTD = zenith total delay; ZHD = zenith hydrostatic delay; ZWD = zenith wet delay.

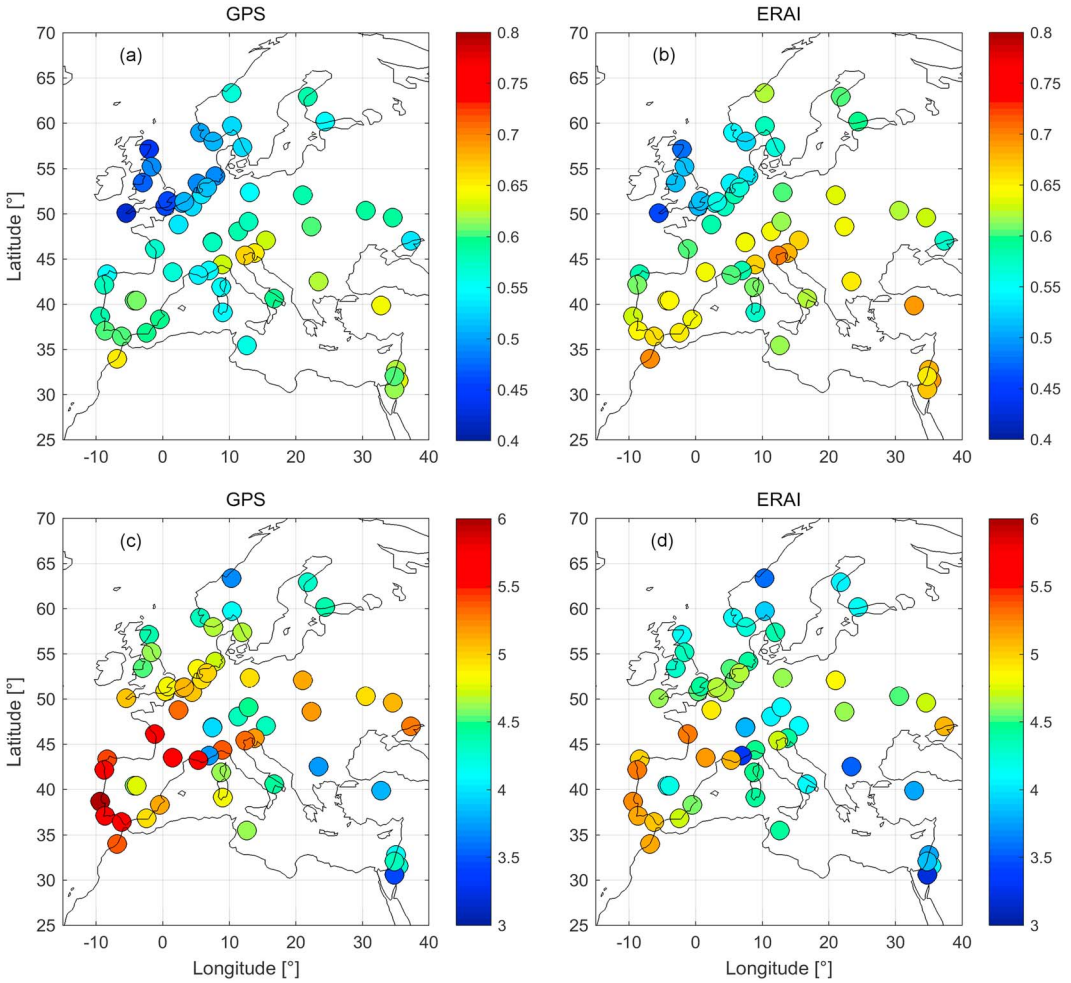

Figure 14. Comparison of (a, b) 1-lag autocorrelation of ZTD residuals (high-frequency component) from GPS and ERAI and (c, d) the standard deviations σ_N from a zero mean Gaussian distribution (Figure 15). ZTD = zenith total delay; GPS = Global Positioning System; ERAI = ERA-Interim.

statistically significant PWV trends, while the stations in Central/East Europe (encircled by black rings, 55%) show statistically significant positive PWV trends. However, when we used the AR(1) model and obtained the 1-lag autocorrelation, it becomes clear that daily PWV time series show high 1-lag correlation coefficients (Figure 9a) stemming from the temporal correlation in the high-frequency component since the weather condition normally extends over multiple days. The PWV 1-day lag correlation coefficients vary between 0.45 and 0.8, and they are correlated with, but slightly smaller than, the values for the temperature (not shown). Smaller values are observed for the stations in the United Kingdom, which is known by its distinct weather that changes rapidly over the hours and days reducing the temporal correlation in temperature and PWV data. This autocorrelation makes the effective sample size significantly smaller than the real sample size (6,940 daily data points) as observed from Figure 9b). In the south (Mediterranean climate), where the PWV shows the greatest 1-lag autocorrelation, the effective sample size is the smallest.

Therefore, this factor, r_1, should not be neglected when estimating the uncertainty σ_b and the confidence intervals for the estimated trends (Tiao et al., 1990). This is done by using a first-order autoregressive model to describe N rather than relying on a white noise process. When r_1 is included in the calculations using equation (11), the standard error increases and the ratio $|b|/\sigma_b$ drops in Figure 9d compared to Figure 8b, which increases the width of the confidence intervals. Hence, the number of stations that show a significant trend decreases to 27% of the stations, Figure 9c. The increase in σ_b depends on the autocorrelation in the time series, which in turn depends on the temporal resolution of the time series and the geographic location of the station; therefore, the increment in σ_b compared to σ_b^* is variable. For daily data, where r_1 is in the

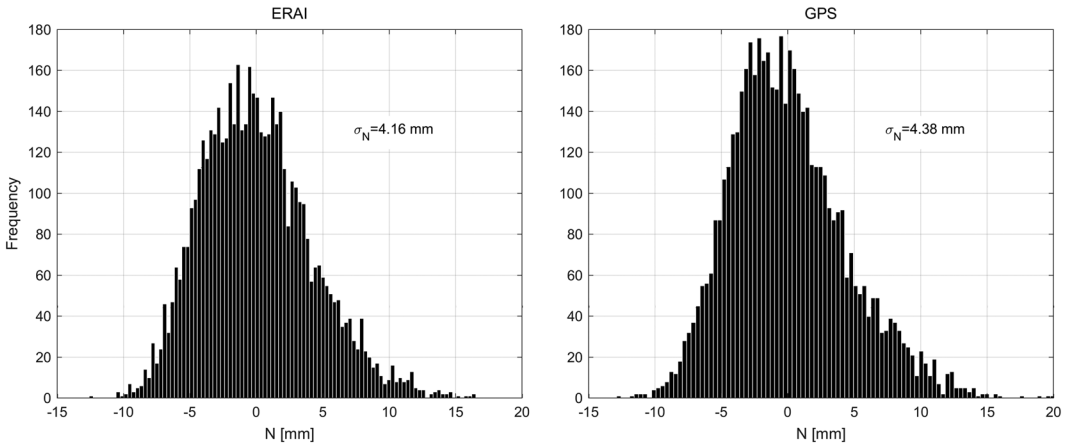

Figure 15. The residuals of the PWV, at station ABER (2.0802°W, 57.144°N], after removing the seasonal and trend components. The standard deviation dependent of the geographic location of the specific site as observed from Figures 14c and 14d. PWV = precipitable water vapor; ERAI = ERA-Interim; GPS = Global Positioning System.

range 0.45–0.8, σ_b can be 1.6 to 2.5 times σ_b^* as shown in Figure 10. This increment was also presented by Weatherhead et al. (1998). Using hourly data, σ_b when using the autoregressive model is 5 to 14 times higher than the case of using the simple white noise model as presented by Klos et al. (2018). These results confirm the necessity of using the autoregressive model instead of a white noise process when assessing the significance of the estimated climatic trends.

The PWV trends over Europe are mainly positive, which agrees with the results presented by Wang et al. (2016) who analyzed the time intervals 1988–2011 and 1995–2011. Mieruch et al. (2008) also observed increasing PWV trends over Central and East Europe in the interval 1996–2005. Durre et al. (2009) showed that the tropospheric water vapor content has been increasing over the Northern Hemisphere as a whole with an average trend of +0.45 mm/decade. Except for some stations on the Atlantic coast, the temperature time series exhibit positive trends, which show 69% spatial correlation with the PWV trends.

As mentioned earlier, the idea was to estimate the ZTD trend as a measure for the PWV trend assuming that the ZHD time series do not show linear trends. Figure 11 shows the magnitudes of the linear trends estimated from 19-year (1996–2014) ERAI-based ZTD, ZHD, and ZWD (related to the PWV trends by the factor $1/Q$ in equation (3) time series. It is clear that the ZTD trend in Figure 11a is not identical to the ZWD trend Figure 11c since the ZHD shows nonzero trends that are negative for the vast majority of the stations. The ZHD trend should be proportional to the air pressure trend, which should according to equation (2) be in the approximate range of −0.9 to 0.24 hPa/decade given the ZHD trend range −2 to 0.5 mm/decade in Figure 11c. We analyzed homogenized time series (1996–2014) of surface pressure and temperature measurements (http://www.dwd.de/EN/climate_environment/cdc/cdc_node.html). The estimated trends are shown in Figure 12. The temperature trends are mainly positive (at 93% of 367 stations) and increase eastward. The spatial pattern and magnitude of the trends is in agreement with the ERAI results in Figure 8c. Also, the spatial pattern in the temperature trends correlate with the ZWD (and PWV) trends spatial pattern. The trends at 34% of the stations are indicated statistically significant. The air pressure shows negative trends in the west and south of Europe, while the trends tend to increase reaching positive values in the northeast following the spatial variations in the ZHD trends. The trend magnitude at the majority of the stations is in the range −0.9 to 0.24. Only trends at 7% of the stations are indicated statistically significant (surrounded by black circles). Since the air pressure includes the partial water vapor pressure, we postulate that the trends in the air pressure are dominated by the water vapor effect, but it is also possible that the air pressure without the water vapor (dry pressure) is changing over time. In order to better understand this effect and give better explanations to the negative trends in the pressure, measurements of the water vapor pressure should be used to estimate the trends in the air pressure with and without the water vapor component.

Since the change in water vapor pressure is related to the change in temperature as described by the Clausius-Clapeyron relation, Trenberth (2011) presented that the PWV has also increased at rates consistent with Clausius-Clapeyron equation ([7%] for the period 1987–2004). We estimated the percentage change per degree Celsius of the ERAI-based ZTD, ZWD, and ZHD. The results are illustrated in Figure 13. Again, the

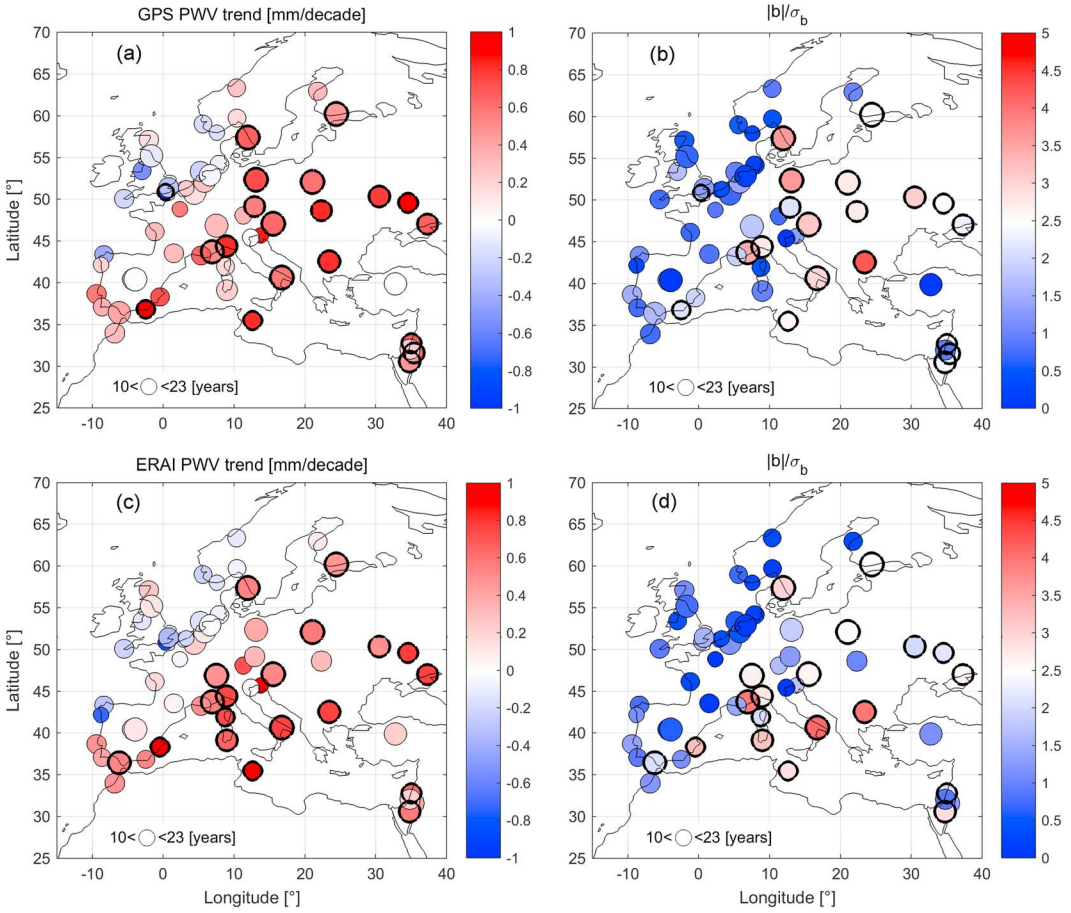

Figure 16. (a–d) Linear trends estimated from GPS PWV time series and the corresponding trends from ERAI PWV data. The statistically significant ($\frac{|b|}{\sigma_b}$) estimate is encircled in black. The size of the marker is proportional to the length of the time series, which goes from 10 to 22 years. GPS = Global Positioning System; PWV = precipitable water vapor; ERAI = ERA-Interim.

percentage change in ZTD per 1° increase in temperature is not identical to the ZWD change since the ZHD also shows a change with the temperature increase, Figure 13. Using 19 years of data (1996–2014), we observed an increase of 3–8%K^{-1} of the ZWD (water vapor) as illustrated Figure 13c, which is generally in agreement with the Clausius-Clapeyron relation. The stations in the south that show more stable weather (higher autocorrelation, Figure 9a) show smaller percentage change, while higher values are observed over the United Kingdom where the weather is highly variable (lower autocorrelation, Figure 9a). The ZTD in Figure 13c shows a positive percentage change of 0.1–0.5%/K. The magnitude is significantly smaller because the ZWD contributes to less than 10% of the ZTD. This explains the drop in the percentage change but not the slight change in the spatial pattern of the ZTD percentage change compared to the ZWD (0.92 spatial correlation). The percentage change in the ZHD (air pressure) with the temperature in Figure 13b shows a ZHD change of −0.06 to 0.06%/K. The spatial pattern in Figure 13b matches that in Figure 13c for the ZWD, which might mean that the change in the ZHD with the temperature is basically caused by the water vapor effect in the air pressure.

4.1.2. GPS Time Series

The next step is to estimate the linear trends from GPS data at the TIGA stations that have data profiles longer than 10 years. We applied the same procedure to the PWV estimates from GPS data processing and included the 1-lag correlation in the calculation of the σ_b and 95% confidence intervals. There is a strong linear correlation of the *N* component at 1-day lag in both GPS and ERAI data, as observed from Figures 14a and 14b. However, GPS-based PWV residuals generally show a smaller 1-lag correlation coefficients than the ERAI data. This indicates that the residuals signal *N* in equation (5) shows higher randomness for the GPS data than ERAI. As we explained earlier, the temporal resolution of the GPS data that are averaged to obtain daily data is 1 hr

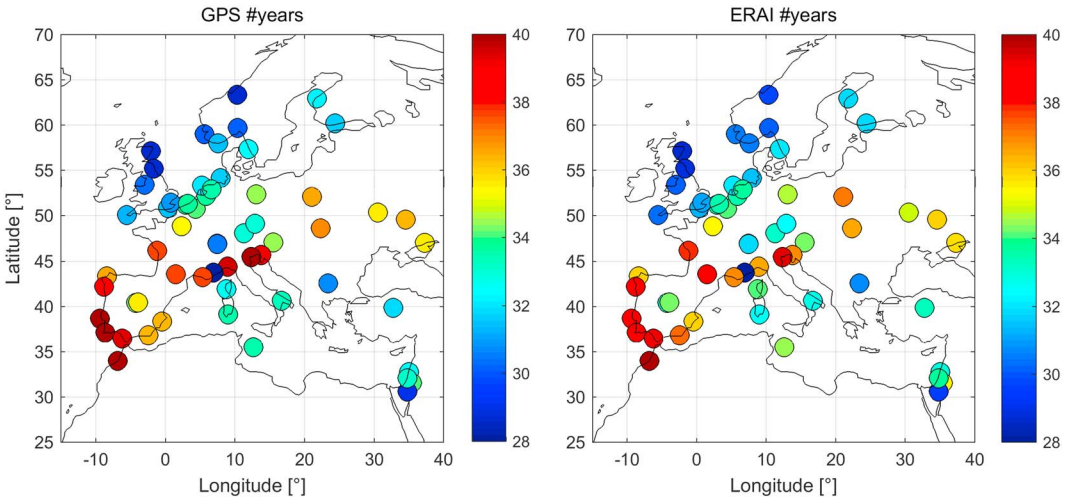

Figure 17. The number of years of daily data required to estimate a trend of 0.3 mm/decade in the PWV data, considering the presence of autocorrelation. PWV = precipitable water vapor; GPS = Global Positioning System; ERAI = ERA-Interim.

higher from the 6-hourly ERAI resolution and the temporal averaging effect in GPS data is smaller. Also, this might indicate the presence of a noise effect in the GPS data. By analyzing the standard deviations for PWV residuals, σ_N, at the GPS stations, they are slightly higher than the corresponding ERAI values as shown in Figures 14c and 14d. It is noticed that both σ_N and the autocorrelaton depend on the location of the GPS station. An example of station ABER (2.0802°W, 57.144°N) in Figure 15 shows the histograms for N from GPS and ERAI, where the standard deviations are 4.38 and 4.16 mm, respectively.

Estimating the linear trends from seasonally adjusted GPS and the corresponding ERAI PWV time series provides the results in Figure 16. We observe that the PWV trends increase, in the eastern and southeastern directions with 83% correlation between GPS and ERAI estimates. For the available data, the estimated trend is indicated significant at 95% confidence level for a few stations ($|b|/\sigma_b > 2$, with σ_b calculated from equation (11). Due to the difference in the σ_N and 1-lag autocorrelation values, the two data sets show different indications of trend significance.

We can see from Figures 14a and 14c that the stations that have higher σ_N and autocorrelation values have a higher trend uncertainties and hence smaller $|b|/\sigma_b$ (unless the trend magnitude is high), which identifies the trend as insignificant. If we increase the length of the data set, the uncertainty should decrease as observed from equation (11). The PWV trends are positive at 86% of the stations regardless of the time interval and the data set that was analyzed. This agrees with the conclusions presented by Wang et al. (2016) who presented a global over land and ocean analysis.

4.2. Required Data Length

It is then expected to study the number of years required to estimate a significant trend from daily ZTD data. Given the standard deviation σ_N, we obtained the sample length of the data that is required to estimate a significant trend using equation (13). Wang et al. (2016) analyzed the PWV trend using data from GPS, radiosondes, and microwave radiometers in three different time intervals from 1973 to 2011. They observed water vapor trends with global mean 0.26, 0.24, and 0.34 mm/decade, respectively. This can roughly be converted into ZWD trends of 1.7–2.2 mm/decade (using a conversion factor of 6.5). In our results of Figure 9, the average PWV trend over Europe is 0.35 mm/decade. For trends above $b = 0.3$ mm/decade, the number of years of daily data is shown in Figure 17. The number of years correlates with the variance of the PWV residual signal and the 1-lag correlation coefficient shown in Figure 14. As we explained above, the required data length, that is, number of years, will be smaller for a higher trend value.

4.3. Tropospheric Gradient Trends

So far we analyzed the ZTD trends and for completeness we also investigated the tropospheric gradient trends. Similar to the ZTD time series, gradient time series also show 1-lag autocorrelation, however, in a smaller magnitude. By estimating the trend using 10-year time series (2005–2014) from GPS and ERAI (10-year data for all stations), we obtained the trends shown in Figures 18a and 18d. The GPS ZTD trends show a spatial

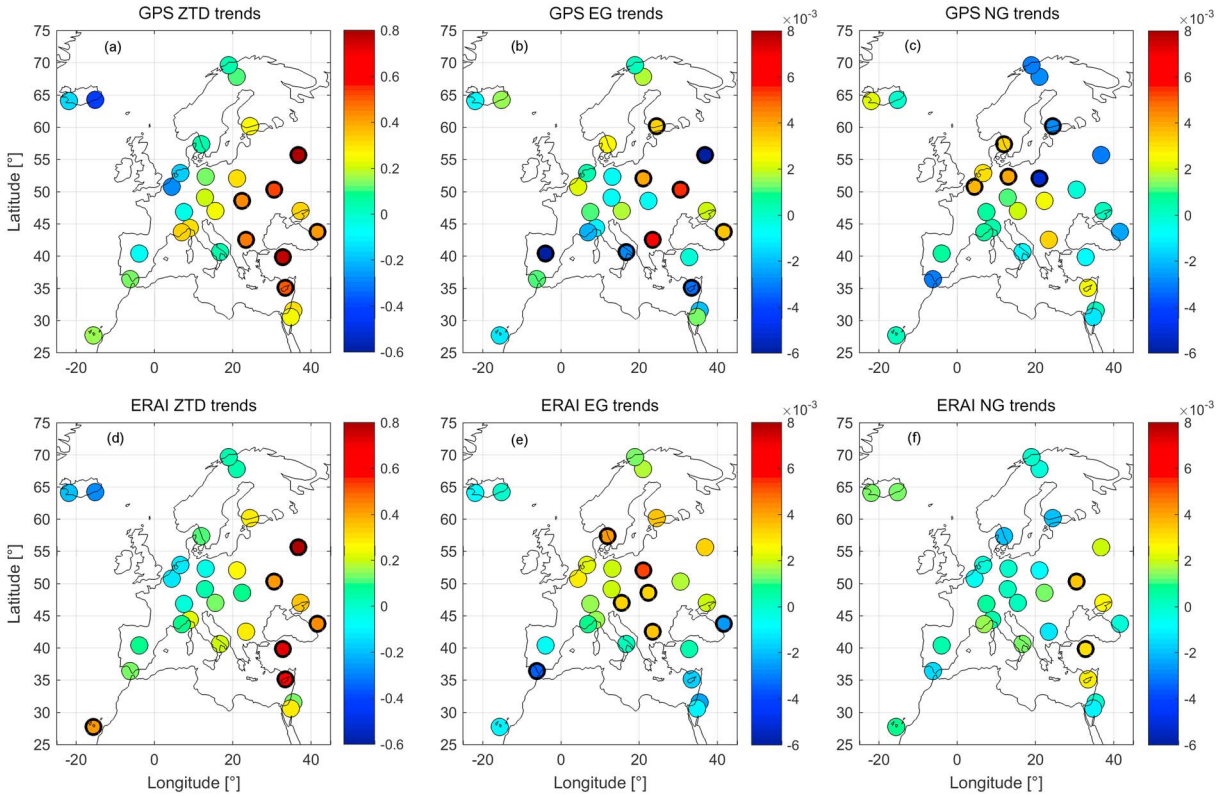

Figure 18. Comparison of estimated (a, d) ZTD trends, (b, e) EW gradient trend, (c, f) NS gradient trends in millimeters per year from GPS and ERAI, respectively. The time series are 10 years long (2005–2014). The significant estimates (autocorrelation considered) are encircled in black. ZTD = zenith total delay; EW = east-west; NS = north-south; GPS = Global Positioning System; ERAI = ERA-Interim.

pattern such that the magnitude increases eastward and so do the ERAI ZTD trends with 96% spatial correlation. Unlike the ZTD trends, we found that the GPS tropospheric gradient trends show poor correlation with the ERA gradient trends, Figures 18b, 18e, 18c, and 18f. While the ERAI gradient trends show smooth variations in space, the GPS gradient trends show higher spatial variations. We do not expect spatial correlation of gradient time series or trends for stations that are hundreds of kilometers apart, but we expect to observe a specific pattern that might support or complete the information we receive from the ZTD trends. We observe high variability in the GPS gradients trends compared to the ZTD trends. This might be due to the site-specific weather conditions that are captured in the GPS data but not by ERAI due to its coarse spatial resolution or the noise in the GPS data.

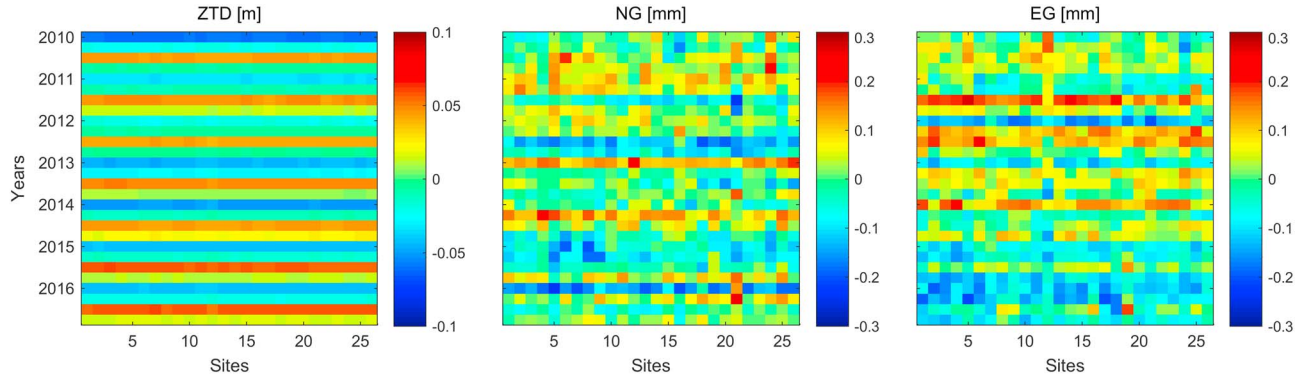

Figure 19. Zero-mean time series of ZTD, EW, and NS gradients averaged quarterly to obtain a value per season (four values/year) for 26 GPS sites in Germany. ZTD = zenith total delay; EW = east-west; NS = north-south; GPS = Global Positioning System.

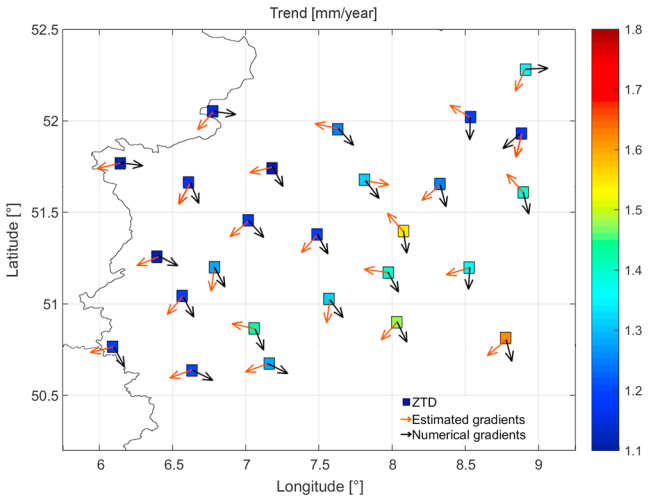

Figure 20. Trends estimated from the ZTD time series in Figure 19. The red arrows show the trends estimated from the gradient time series in Figure 19, and the black arrows show the trends of the numerically approximated gradients from the ZTD. ZTD = zenith total delay.

We checked the ZTD and gradient trends for stations of a region in western Germany, where 26 national stations are separated by an average distance of 30 km (Alshawaf et al., 2017). We used 7-year time series (2010–2016), and in order to avoid high temporal variations caused by weather variability, we averaged the data such that a value is available for each season (four estimates/year). One should bear in mind here that the goal of using these time series, despite being short, is to compare the ZTD and tropospheric gradients at closely mounted sites and not to estimate significant climatic trends. Figure 19 shows the ZTD, NS, and EW gradient time series (anomalies) for all stations. While the ZTD time series are highly correlated in space, the gradient data do not show a similar correlation. Regardless of the short distance between adjacent stations and the highly smoothing of the data, the gradient (both EW and NS) time series at neighboring stations still show poor correlation. This might mean that 30-km separating distance is not adequately short to show correlation in the gradient time series or it might be that the GPS gradient data still have a high noise influence. Another important point here is the homogeneity of the gradient time series. It is more critical to assess their homogeneity or successfully detect inhomogeneities in the gradients compared to the ZTD time series due to their small magnitudes. There is a probability that a point is indicated to be a change point as a false alarm or a change point is missed.

In Appendix B, we show that there is a relation between the ZTD gradients (the derivative of ZTD along the longitude and latitude directions) and the tropospheric gradients. We also show that the same relation holds true for the ZTD gradient trends and the tropospheric gradient trends. We made use of this relation to show if it is applicable to the GPS tropospheric estimates. In Figure 20, the little squares show the ZTD trends, while the arrows show the gradients trends. The red arrows show the trend estimated from the EW and NS GPS tropospheric gradients, and the black arrows show the trends of the numerically approximated gradients (ZTD gradients). There is a big difference, almost no correlation, between the two methods: the trends estimated from the tropospheric gradients and ZTD gradients. The black arrows in Figure 20 mostly point to the southeastern direction indicating a positive east gradient and a negative north gradient. The red arrows do not show a similar consistency. The ZTD trends show smooth variations in space with a tendency to increase in the southeast, while the gradient trends do not show a specific pattern. It might be safe to say that the tropospheric gradient time series, in their current state, do still have a noise influence or inhomogeneities that are difficult to be detected due to the magnitude of the gradients that makes it difficult to derive trustworthy trends.

5. Conclusions

In this paper, (1) we analyzed the quality of the tropospheric products, ZTD, PWV, and gradients estimated from the TIGA network GPS data in Europe and prepared the time series for trend estimation. (2) We identified the statistical significance of the estimated trends taking into account the temporal autocorrelation of the tropospheric time series by using a first-order autoregressive model AR(1) for the residuals (after removing

the trend and seasonal components from the time series) instead of a white noise process. The AR(1) model provides realistic trend uncertainty estimates, while the white noise model does not, and hence, it should not be used to evaluate the significance of climatic trends. (3) We approximated, based on the used first-order autoregressive model, the number of years of daily data required to estimate a statistically significant trend. (4) We derived the percentage change of tropospheric ZTD, ZHD, and ZWD per 1 ° Celsius increase in temperature. (5) We compared the gradient and gradient trends estimated from GPS and ERAI data sets.

Should the time series have gaps shorter that 1.5 years, a first-order autoregressive model is applied for closing the gaps and providing a continuous time series for the purpose of trend estimation. Longer gaps can of course be filled in a similar way; however, we do not recommend using time series with gaps longer than 1.5 years since the statistical properties of the time series change after the gap filling and hence the estimated trend. It is uncontroversial that the homogeneity of the time series has to be checked prior to the trend estimation. To estimate the significance of the estimated trend, the autocorrelation in the atmospheric time series (PWV, ZTD, temperature, pressure, etc.) has to be considered in the calculation of the standard error. Therefore, a first-order autoregressive model was found to be more useful than a white noise process, the latter underestimates the standard error. For daily data, the trend uncertainty estimated using an AR(1) model is 1.6–2.5 times the standard error estimated assuming a white noise process. The value depends on the autocorrelation and noise standard deviation, which in turn depend on the location of the GPS station. This factor should decrease if monthly data are used.

The results mainly show positive PWV (or ZWD) trends in Europe with only a few stations on the western coast that show trends below zero. About 27% of the GPS stations show significant, positive PWV trends that increase in the south and eastern Europe. The trends were estimated from the GPS data in different time intervals (10–22 years). Using 19-year ERAI data (1996–2014), the PWV trend at eight stations of 193 is slightly below zero (not significant), while at the remaining stations the trend is positive and below 1 mm/decade. The PWV trends show 69% spatial correlation with temperature trends. It is not only the ZWD (PWV) time series that show trend over time but also the ZHD time series. They show mainly negative trends that correlate with the trends estimated from surface pressure measurements. However, the trends in the ZHD were not indicated statistically significant. The PWV (represented by ZWD) shows a percentage change of 3–8%/° C increase in temperature with the higher values observed in the western coast, particularly over United Kingdom.

We found that the number of years of daily data required to estimate a PWV trend above 0.3 mm/decade is between 28 and 40 years. This number increases when the high-frequency component (stochastic) has high standard deviations and when the 1-lag correlation coefficient of the time series is high. Therefore, for stations in the north, 28 years of daily data are adequate, while 40 years are required in the southwest. While the ZTD trends from GPS and ERAI show high correlation, we did not observe such correlation in the tropospheric gradients.

It is required to put a focus on the reprocessing of the GPS data such that the gaps are avoided or at least highly reduced. In the future work, we are going to analyze partial vapor pressure and find its relation to the PWV, pressure, and temperature trends. Using these measurements, it is required to check if the air pressure would still show trends if the vapor pressure was subtracted. It is also important to check the relation of PWV trends with tropospheric temperature trends rather than the surface temperature trends. According to Wang et al. (2016), the PWV trends should show more correlation with tropospheric temperature.

Appendix A

Assuming the component N in equation (5) follows a first-order autoregressive model AR(1), that is, $N_t = r_1 N_{t-1} + \epsilon$, the standard error of the trend estimated by the least squares linear regression is obtained from the following:

$$\sigma_b = \frac{\sigma_\epsilon}{(1 - r_1)\sqrt{\sum_{t=1}^{n}(t - \bar{t})^2}} = \frac{\sigma_N\sqrt{1 - r_1^2}}{(1 - r_1)\sqrt{\sum_{t=1}^{n}(t - \bar{t})^2}}$$

$$= \sigma_N \sqrt{\frac{(1-r_1)(1+r_1)}{(1-r_1)^2}} \frac{1}{\sqrt{\sum_{t=1}^{n}(t-\bar{t})^2}}$$
$$= \frac{\sigma_N}{\sqrt{\sum_{t=1}^{n}(t-\bar{t})^2}} \sqrt{\frac{1+r_1}{1-r_1}} \quad \text{(A1)}$$

with n the sample size (number of data points). Given that $\sum_{t=1}^{n}(t-\bar{t})^2 = n(n^2-1)/12 \approx n^3/12$ for $n \gg 1$; therefore, σ_b for the trend estimated in millimeters per year from monthly data is obtained using (Tiao et al., 1990; Weatherhead et al., 1998) the following:

$$\sigma_b = \frac{\sigma_N}{n_y^{3/2}} \sqrt{\frac{1+r_1}{1-r_1}} \quad \text{(A2)}$$

with n_y is the number of years of monthly data ($n_y = n/12$). For daily data, the formula is slightly different, that is,

$$\sigma_b = \frac{\sigma_N}{\sqrt{\frac{n^3}{(365)^2 \cdot 12}}} \sqrt{\frac{1+r_1}{1-r_1}} \quad \text{(A3)}$$

The 1-lag autocorrelation, r_1, is estimated from the following:

$$r_1 = \frac{\sum_{t=2}^{n} \hat{N}_{t-1}\hat{N}_t}{\sum_{t=2}^{n} \hat{N}_{t-1}^2} \quad \text{(A4)}$$

The ratio $|b|/\sigma_b$ defines the confidence in the estimated trend. According to Tiao et al. (1990), the likelihood of detecting a trend b_o is at least 90% if $|b_o|/\sigma_b > 3.3$. For a probability of 95%, the ratio increases such that $|b_o|/\sigma_b > 3.64$. Starting from equation (A1), we want to estimate the sample size required to achieve a given significance level. Dividing both sides by $|b_o|$ we get the following:

$$\frac{\sigma_b}{|b_o|} = \frac{1}{|b_o|} \frac{\sigma_N}{\sqrt{\sum_{t=1}^{n}(t-\bar{t})^2}} \sqrt{\frac{1+r_1}{1-r_1}}$$
$$\frac{\sigma_b}{|b_o|} = \frac{\sigma_N \sqrt{12}}{|b_o|\, n^{3/2}} \sqrt{\frac{1+r_1}{1-r_1}} \quad \text{(A5)}$$

for the number of data points, n, $\sum_{t=1}^{n}(t-\bar{t})^2 = n(n^2-1)/12 \approx n^3/12$ for $n \gg 1$. Solving for n, we obtain the following:

$$n = \left[\frac{|b_o|}{\sigma_b} \frac{\sigma_N}{|b_o|} \sqrt{12} \sqrt{\frac{1+r_1}{1-r_1}} \right]^{2/3} \quad \text{(A6)}$$

For 90% confidence, $|b_o|/\sigma_b = 3.3$, then

$$n = \left[3.3 \sqrt{12} \frac{\sigma_N}{|b_o|} \sqrt{\frac{1+r_1}{1-r_1}} \right]^{2/3} \quad \text{(A7)}$$

To get the number of years n_{req} for monthly data, dividing both sides by 12 gives

$$n_{\text{req}} = \left[3.3 \frac{\sigma_N}{|b_o|} \sqrt{\frac{1+r_1}{1-r_1}} \right]^{2/3} \quad \text{(A8)}$$

with σ_N in millimeters and b_o in millimeters per year. To get the number of years from daily data, we divide equation (A7) by 365.25, then

$$n_{\text{req}} = \left[3.3 \frac{\sqrt{12}}{\sqrt{365.25}} \frac{\sigma_N}{|b_o|} \sqrt{\frac{1+r_1}{1-r_1}} \right]^{2/3} \quad \text{(A9)}$$

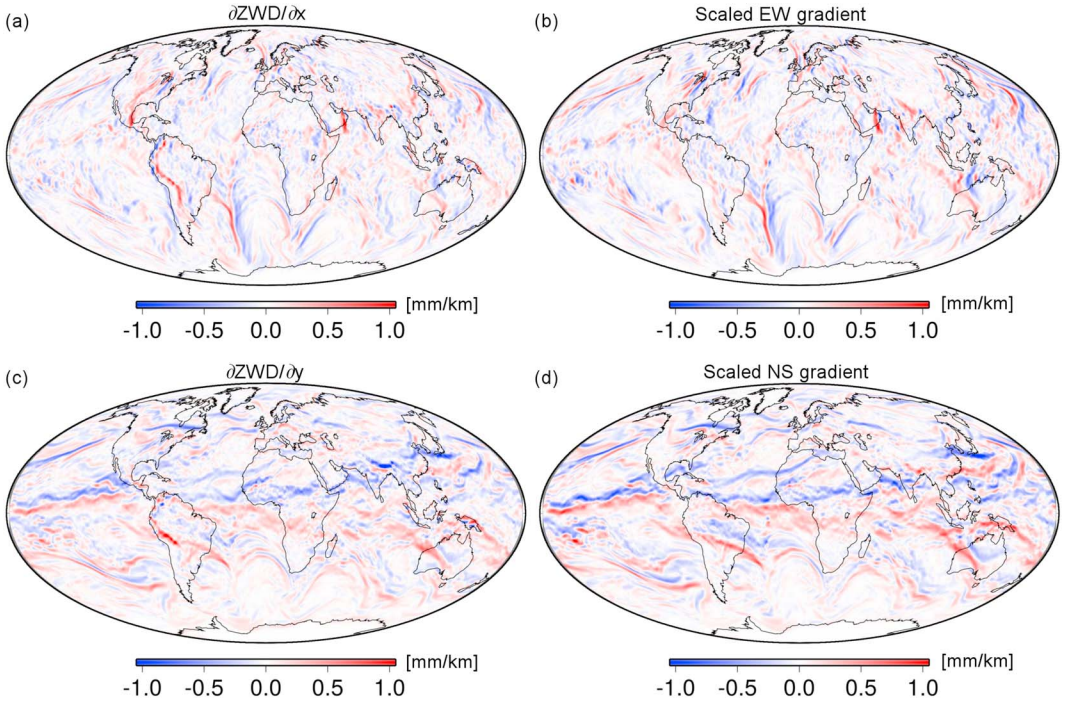

Figure B1. Comparison between (a, b) the EW nonhydrostatic gradient obtained to emulate the GPS estimates by ray tracing of ERAI data on 31 May 2013, 6:00 UTC and those who are numerically approximated from ZWD data ($\partial ZWD/\partial x$). In (c, d) are the NS ray traced tropospheric gradients and numerically obtained gradients ($\partial ZWD/\partial y$). The tropospheric gradients are scaled using a constant scale height of 3 km. EW = east-west; GPS = Global Positioning System; ERAI = ERA-Interim; ZWD = zenith wet delay; NS = north-south.

with σ_N in millimeters and b_o in millimeters per year (therefore, the above equation has only the $\sqrt{365.25}$ and not $365.25^{3/2}$). For 95% confidence, the 3.3 factor in the above equations is replaced by 3.64.

Appendix B

Ruffini et al. (1999) showed that the estimated tropospheric EW and NS gradients should roughly be proportional to ZTD gradients, that is, $\mathbf{G} = H\mathbf{Z}$ with $\mathbf{G}$ the vector of EW and NS tropospheric gradients and $\mathbf{Z}$ is the numerical gradients from the ZTD data. The scaling factor, H, depends on the vertical structure of the atmosphere and is found to be about 1.31 km for a station network in the area of Madrid (Spain). This value of the scaling factor (scale height) should, of course, vary with the geographic location and time. We studied the relationship between the tropospheric gradients and ZTD from global ERA-interim data. As presented by Zus et al. (2012), we first utilized ERAI refractivity fields to produce maps of ZTD, ZHD, and ZWD at 1° × 1° spatial resolution. For each grid point we derived the tropospheric EW and NS gradients from ray traced tropospheric delays.

We refer to the spatial gradients calculated from ZTD, that is, $\partial ZTD/\partial x$ and $\partial ZTD/\partial y$, as ZTD gradients, while the EW and NS gradients as tropospheric gradients. We calculated the ZTD gradients in the eastward and poleward directions by finite differencing, as follows. For gridded data, the gradient can be numerically approximated by one-sided forward difference, that is,

$$f'(x) = \frac{f(x+h) - f(x)}{h} \tag{B1}$$

or central difference

$$f'(x) = \frac{f(x+h) - f(x-h)}{2h} \tag{B2}$$

For scattered data, f can be extended by a Taylor expansion such that

$$f_i = f_0 + \Delta\mathbf{x}_i^T \nabla f_0 + r_i \tag{B3}$$

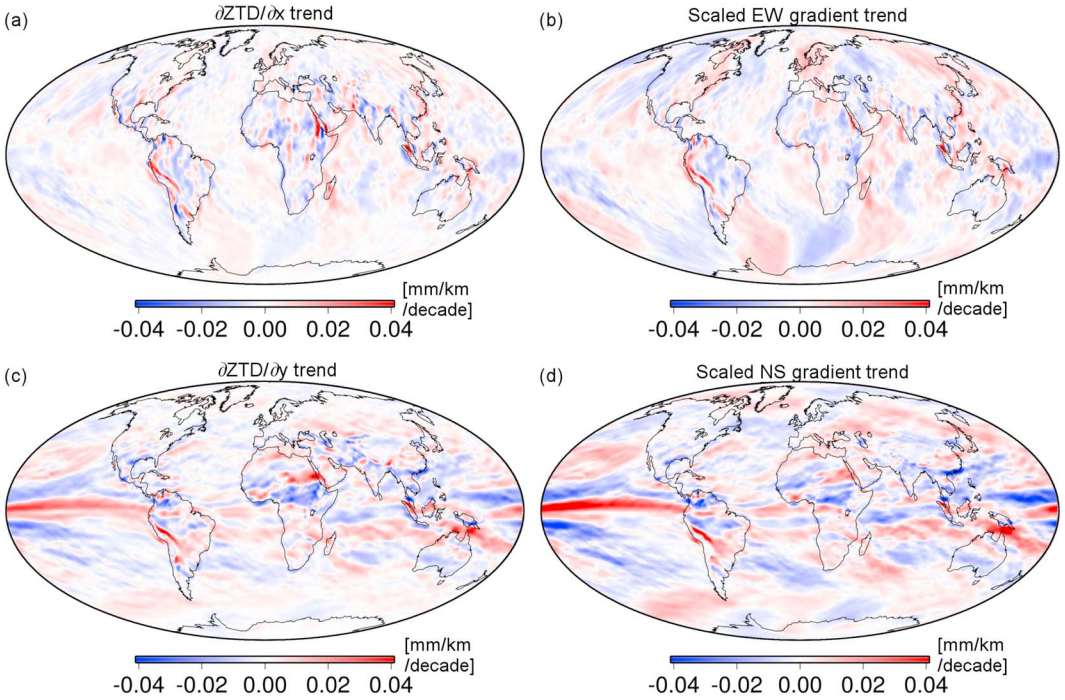

Figure B2. (a–d) The linear trend estimated from 19-year data of ray traced gradients (scaled by *H*) and the corresponding numerically approximated gradients from ZTD data (ZTD gradients). ZTD = zenith total delay; EW = east-west; NS = north-south.

where f_0 and ∇f_0 are the function the gradients at $\mathbf{x}_0$. For ZTD, for example,

$$\mathrm{ZTD}(x_i, y_i) = \mathrm{ZTD}(x_0, y_0) + [\Delta x_i \quad \Delta y_i]\,[eg \quad ng]^T + r(x_i, y_i) \tag{B4}$$

where $\Delta x_i = x_i - x_0$ and $\Delta y_i = y_i - y_0$ and *eg* and *ng* are the gradient components. We can solve for *eg* and *ng* using least squares adjustment.

When compared to the tropospheric gradients, we observed a strong correlation. The correlation coefficients for the grids in Figure B1 are 0.83 for the NS gradient and 0.81 for the EW gradient, which could probably be improved by adjusting the scaling factor for different regions (in this work, the scale height is fixed to 3 km). We extended the analysis to check whether the trends show a similar proportional relation, which turned out to be true. Namely, the ZTD gradient trends, estimated for the period 1996–2014, are proportional to the tropospheric gradient trends as shown in Figure B2. This suggests that the tropospheric gradient trends can give supportive information about the spatial variations of the ZTD trends.

We proceeded to numerically approximate the ZWD gradients by one-sided difference of the ZWD grids in the NS and EW directions. By comparing the two grids, we observed a strong correlation between the ray tracing-based gradient grids and the numerically derived gradients. The correlation coefficients for the grids in Figure B1 are 0.83 for the NS gradient and 0.81 for the EW gradient, which should be improved by adjusting the height scale for different regions.

We extended the analysis to check if the trends show a similar proportional relation, which according to our results turned out to be true. Namely, the numerically derived EW and NS gradients of the ZTD trends, estimated for the period 1996–2014, are proportional to the ray tracing-based gradient trends as shown in Figure B2. This suggests that the tropospheric gradients, when accurate, can give supportive information about the spatial variations of the zenith path delay and climatic trends.

Acknowledgments
The authors would like to thank the ECMWF for making publicly available the ERA-Interim data. We would also like to thank the German Weather Service (DWD) for providing the synoptic data. All the data used are listed in the references or archived in http://www.dwd.de/EN/climate_environment/cdc/cdc_node.html and http://apps.ecmwf.int/datasets/data/interim-full-daily/levtype=sfc/ repository.

References

Akaike, H. (1969). Fitting autoregressive models for prediction. *Annals of the institute of Statistical Mathematics*, *21*(1), 243–247.
Alshawaf, F., Balidakis, K., Dick, G., Heise, S., & Wickert, J. (2017). Estimating trends in atmospheric water vapor and temperature time series over Germany. *Atmospheric Measurement Techniques*, *10*(9), 3117.

Alshawaf, F., Fuhrmann, T., Knopfler, A., Luo, X., Mayer, M., Hinz, S., & Heck, B. (2015). Accurate estimation of atmospheric water vapor using GNSS observations and surface meteorological data. *IEEE Transactions on Geoscience and Remote Sensing*, *53*(7), 3764–3771. https://doi.org/10.1109/TGRS.2014.2382713

Balidakis, K., Nilsson, T., Zus, F., Glaser, S., Heinkelmann, R., Deng, Z., & Schuh, H. (2018). Estimating integrated water vapor trends from VLBI, GPS, and numerical weather models: Sensitivity to tropospheric parameterization. *Journal of Geophysical Research: Atmospheres*, *123*, 6356–6372. https://doi.org/10.1029/2017JD028049

Bar-Sever, Y. E., Kroger, P. M., & Borjesson, J. A. (1998). Estimating horizontal gradients of tropospheric path delay with a single GPS receiver. *Journal of Geophysical Research*, *103*(B3), 5019–5035.

Bender, M., Dick, G., Wickert, J., Schmidt, T., Song, S., Gendt, G., et al. (2008). Validation of GPS slant delays using water vapour radiometers and weather models. *Meteorologische Zeitschrift*, *17*(6), 807–812.

Bengtsson, L., Hagemann, S., & Hodges, K. I. (2004). Can climate trends be calculated from reanalysis data? *Journal of Geophysical Research*, *109*, D11111. https://doi.org/10.1029/2004JD004536

Bevis, M., Businger, S., Herring, T. A., Rocken, C., Anthes, R. A., & Ware, R. H. (1992). GPS meteorology: Remote sensing of atmospheric water vapor using the global positioning system. *Journal of Geophysical Research*, *97*(D14), 15,787–15,801.

Chen, G., & Herring, T. (1997). Effects of atmospheric azimuthal asymmetry on the analysis of space geodetic data. *Journal of Geophysical Research*, *102*(B9), 20,489–20,502.

Dee, D. P., Uppala, S. M., Simmons, A. J., Berrisford, P., Poli, P., Kobayashi, S., et al. (2011). The ERA-Interim reanalysis: Configuration and performance of the data assimilation system. *Quarterly Journal of the Royal Meteorological Society*, *137*(656), 553–597. https://doi.org/10.1002/qj.828

Deng, Z., Gendt, G., & Schöne, T. (2015). Status of the IGS-TIGA tide gauge data reprocessing at GFZ . In *Proceedings of the IAG Scientific Assembly 143, Postdam, Germany, 1-6 September, 2013* (pp. 33–40). Switzerland: Springer.

Douša, J., Dick, G., Kačmařík, M., Brožková, R., Zus, F., Brenot, H., et al. (2016). Benchmark campaign and case study episode in central Europe for development and assessment of advanced GNSS tropospheric models and products. *Atmospheric Measurement Techniques*, *9*(7), 2989–3008. https://doi.org/10.5194/amt-9-2989-2016

Durre, I., Williams, C. N., Yin, X., & Vose, R. S. (2009). Radiosonde-based trends in precipitable water over the Northern Hemisphere: An update. *Journal of Geophysical Research*, *114*, D05112. https://doi.org/10.1029/2008JD010989

Gendt, G., Dick, G., Reigber, C., Tomassini, M., Liu, Y., & Ramatschi, M. (2004). Near real time GPS water vapor monitoring for numerical weather prediction in Germany. *Journal of the Meteorological Society of Japan*, *82*(1B), 361–370.

Gradinarsky, L., Johansson, J., Bouma, H., Scherneck, H.-G., & Elgered, G. (2002). Climate monitoring using GPS. *Physics and Chemistry of the Earth Parts A/B/C*, *27*(4), 335–340.

Haas, R., Elgered, G., Gradinarsky, L., & Johansson, J. M. (2003). Assessing long term trends in the atmospheric water vapor content by combining data from VLBI, GPS, radiosondes and microwave radiometry. In W. Schwegmann & V. Thorandt (Eds.), *Proceedings of the 16th Working Meeting on European VLBI for Geodesy and Astrometry* (pp. 279–288). Frankfurt/Leipzig: Bundesamt für Kartographie und Geodäsie.

Hausmann, P., Sussmann, R., Trickl, T., & Schneider, M. (2017). A decadal time series of water vapor and D/H isotope ratios above Zugspitze: Transport patterns to central Europe. *Atmospheric Chemistry and Physics Discussions*, *2017*, 7635–7651. https://doi.org/10.5194/acp-2016-1029

Jade, S., & Vijayan, M. (2008). GPS-based atmospheric precipitable water vapor estimation using meteorological parameters interpolated from NCEP global reanalysis data. *Journal of Geophysical Research*, *113*, D03106. https://doi.org/10.1029/2007JD008758

Killick, R., Fearnhead, P., & Eckley, I. A. (2012). Optimal detection of change points with a linear computational cost. *Journal of the American Statistical Association*, *107*(500), 1590–1598.

Klos, A., Hunegnaw, A., Teferle, F. N., Abraha, K. E., Ahmed, F., & Bogusz, J. (2018). Statistical significance of trends in zenith wet delay from re-processed GPS solutions. *GPS Solutions*, *22*(2), 51.

Lacis, A. A., Schmidt, G. A., Rind, D., & Ruedy, R. A. (2010). Atmospheric CO_2: Principal control knob governing Earth's temperature. *Science*, *330*, 356–359.

Lavielle, M., & Teyssiere, G. (2006). Detection of multiple change-points in multivariate time series. *Lithuanian Mathematical Journal*, *46*(3), 287–306.

Luo, X., Mayer, M., & Heck, B. (2008). Extended neutrospheric modelling for the GNSS-based determination of high-resolution atmospheric water vapor fields. *Boletim de Ciencias Geodesicas*, *14*(2), 149–170.

Mieruch, S., Noël, S., Bovensmann, H., & Burrows, J. (2008). Analysis of global water vapour trends from satellite measurements in the visible spectral range. *Atmospheric Chemistry and Physics*, *8*(3), 491–504.

Mieruch, S., Schröder, M., Noël, S., & Schulz, J. (2014). Comparison of decadal global water vapor changes derived from independent satellite time series. *Journal of Geophysical Research: Atmospheres*, *119*, 12,489–12,499. https://doi.org/10.1002/2014JD021588

Nilsson, T., & Elgered, G. (2008). Long-term trends in the atmospheric water vapor content estimated from ground-based GPS data. *Journal of Geophysical Research*, *113*, D19101. https://doi.org/10.1029/2008JD010110

Ning, T., Wickert, J., Deng, Z., Heise, S., Dick, G., Vey, S., & Schöne, T. (2016). Homogenized Time Series of the Atmospheric Water Vapor Content Obtained from the GNSS Reprocessed Data. *Journal of Climate*, *29*, 2443–2456.

Pacione, R., Araszkiewicz, A., Brockmann, E., & Dousa, J. (2017). EPN-Repro2: A reference GNSS tropospheric data set over Europe. *Atmospheric Measurement Techniques*, *10*(5), 1689–1705. https://doi.org/10.5194/amt-10-1689-2017

Ruffini, G., Kruse, L., Rius, A., Bürki, B., Cucurull, L., & Flores, A. (1999). Estimation of tropospheric zenith delay and gradients over the madrid area using GPS and WVR data. *Geophysical Research Letters*, *26*(4), 447–450.

Santer, B. D., Wigley, T., Boyle, J., Gaffen, D. J., Hnilo, J., Nychka, D., et al. (2000). Statistical significance of trends and trend differences in layer-average atmospheric temperature time series. *Journal of Geophysical Research*, *105*(D6), 7337–7356.

Schöne, T., Schön, N., & Thaller, D. (2009). IGS tide gauge benchmark monitoring pilot project (TIGA): Scientific benefits. *Journal of Geodesy*, *83*(3-4), 249–261.

Sherwood, S. C., Ingram, W., Tsushima, Y., Satoh, M., Roberts, M., Vidale, P. L., & O'Gorman, P. A. (2010). Relative humidity changes in a warmer climate. *Journal of Geophysical Research*, *115*, D09104. https://doi.org/10.1029/2009JD012585

Simmons, A., Uppala, S., Dee, D., & Kobayashi, S. (2007). ERA-Interim: New ECMWF reanalysis products from 1989 onwards. *ECMWF Newsletter*, *110*, 29–35.

Suarez, M. J., Rienecker, M. M., Todling, R., Bacmeister, J., Takacs, L., Liu, H. C., et al. (2008). The GEOS-5 data assimilation system documentation of versions 5.0. 1, 5.1. 0, and 5.2. 0.

Tiao, G., Reinsel, G., Xu, D., Pedrick, J., Zhu, X., Miller, A., et al. (1990). Effects of autocorrelation and temporal sampling schemes on estimates of trend and spatial correlation. *Journal of Geophysical Research*, *95*(D12), 20,507–20,517.

Trenberth, K. E. (2011). Changes in precipitation with climate change. *Climate Research*, *47*(1-2), 123–138.

Trenberth, K. E., Fasullo, J., & Smith, L. (2005). Trends and variability in column-integrated atmospheric water vapor. *Climate dynamics*, *24*(7-8), 741–758.

Vey, S., Dietrich, R., Fritsche, M., Rülke, A., Steigenberger, P., & Rothacher, M. (2009). On the homogeneity and interpretation of precipitable water time series derived from global GPS observations. *Journal of Geophysical Research*, *114*, D10101. https://doi.org/10.1029/2008JD010415

Wang, J., Dai, A., & Mears, C. (2016). Global water vapor trend from 1988 to 2011 and its diurnal asymmetry based on GPS, radiosonde, and microwave satellite measurements. *Journal of Climate*, *29*(14), 5205–5222.

Weatherhead, E. C., Reinsel, G. C., Tiao, G. C., Meng, X.-L., Choi, D., Cheang, W.-K., et al. (1998). Factors affecting the detection of trends: Statistical considerations and applications to environmental data. *Journal of Geophysical Research*, *103*(D14), 17,149–17,161.

Webley, P. W., Bingley, R. M., Dodson, A. H., Wadge, G., Waugh, S. J., & James, I. N. (2002). Atmospheric water vapour correction to inSAR surface motion measurements on mountains: Results from a dense GPS network on Mount Etna. *Physics and Chemistry of the Earth Parts A/B,/C*, *27*(4-5), 363–370. https://doi.org/10.1016/S1474-7065(02)00013-X

Wigley, T. M., Santer, B., & Lanzante, J. (2006). Appendix A: Statistical issues regarding trends. Temperature trends in the lower atmosphere: Steps for understanding and reconciling differences.

Ye, H., & Fetzer, E. J. (2010). Atmospheric moisture content associated with surface air temperatures over northern Eurasia. *International Journal of Climatology*, *30*(10), 1463–1471.

Zus, F., Bender, M., Deng, Z., Dick, G., Heise, S., Shang-Guan, M., & Wickert, J. (2012). A methodology to compute GPS slant total delays in a numerical weather model. *Radio Science*, *47*, RS2018. https://doi.org/10.1029/2011RS004853